


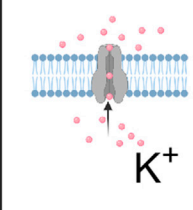

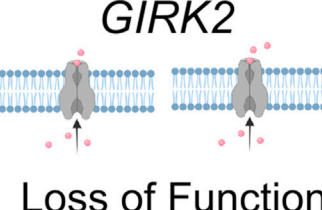
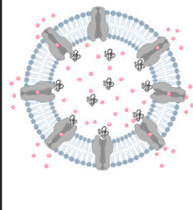
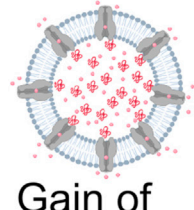
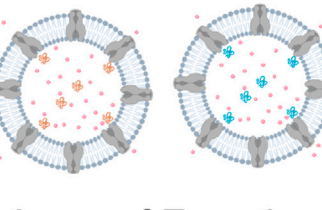


Article

Encephalopathy-causing mutations in Gβ₁ (*GNB1*) alter regulation of neuronal GIRK channels

	Gβ ₁ WT vs mutants		
	Gβ ₁ WT	Gβ ₁ K78R	Gβ ₁ I80N & I80T
Gβ ₁ protein levels	 <p>RNA ↓ Gβ₁ protein</p>	 <p>Gain of Expression</p>	 <p>Partial Loss of Expression</p>
GIRK single channel activity	 <p>K⁺</p>	<p><i>GIRK1/2</i></p>  <p>Partial Loss of Function</p>	<p><i>GIRK2</i></p>  <p>Loss of Function</p>
Whole-cell GIRK currents		 <p>Gain of Function</p>	 <p>Loss of Function</p>
Rescue		GIRK inhibitors	GIRK activators

Haritha P. Reddy, Daniel Yakubovich, Tal Keren-Raifman, ..., Jonathan A. Javitch, Amal K. Bera, Nathan Dascal

haritha89reddy@gmail.com (H.P.R.)
amal@iitm.ac.in (A.K.B.)
dascaln@tauex.tau.ac.il (N.D.)

Highlights
GIRK channels are key players affected by *GNB1* mutations under study (K78R and I80N/T)

Effects of mutations (LoF or GoF) are channel subunit composition-specific

The findings help to understand the *GNB1* encephalopathy and to devise treatments

The results yield new insights into mechanisms of Gβγ regulation of GIRKs

Reddy et al., iScience 24, 103018
September 24, 2021 © 2021 The Author(s).
<https://doi.org/10.1016/j.isci.2021.103018>



Article

Encephalopathy-causing mutations in Gβ₁ (*GNB1*) alter regulation of neuronal GIRK channels

Haritha P. Reddy,^{1,2,*} Daniel Yakubovich,^{1,3} Tal Keren-Raifman,¹ Galit Tabak,¹ Vladimir A. Tsemakhovich,¹ Maria H. Pedersen,^{4,5,6} Boris Shalomov,¹ Sophie Colombo,^{7,10} David B. Goldstein,^{7,8} Jonathan A. Javitch,^{4,5} Amal K. Bera,^{2,*} and Nathan Dascal^{1,9,11,*}

SUMMARY

Mutations in the *GNB1* gene, encoding the Gβ₁ subunit of heterotrimeric G proteins, cause *GNB1* Encephalopathy. Patients experience seizures, pointing to abnormal activity of ion channels or neurotransmitter receptors. We studied three Gβ₁ mutations (K78R, I80N and I80T) using computational and functional approaches. In heterologous expression models, these mutations did not alter the coupling between G protein-coupled receptors to G_{i/o}, or the Gβγ regulation of the neuronal voltage-gated Ca²⁺ channel Ca_v2.2. However, the mutations profoundly affected the Gβγ regulation of the G protein-gated inwardly rectifying potassium channels (GIRK, or Kir3). Changes were observed in Gβ₁ protein expression levels, Gβγ binding to cytosolic segments of GIRK subunits, and in Gβγ function, and included gain-of-function for K78R or loss-of-function for I80T/N, which were GIRK subunit-specific. Our findings offer new insights into subunit-dependent gating of GIRKs by Gβγ, and indicate diverse etiology of *GNB1* Encephalopathy cases, bearing a potential for personalized treatment.

INTRODUCTION

Mutations in *GNB1* cause a neurological disorder (*GNB1* Encephalopathy) characterized by general developmental delay, epileptiform activity in the electroencephalogram (EEG) and/or seizures of several types, muscle hypotonia or hypertonia, and additional variable symptoms (reviewed in Revah-Politi et al., 2020). *GNB1* encodes the ubiquitous Gβ₁ subunit of heterotrimeric G proteins, which mediate G protein-coupled receptor (GPCR) signaling. Gβ is an obligatory dimer with Gγ (Oldham and Hamm, 2006, 2008). There are 5 genes encoding Gβ subunits and 13 for Gγ; Gβ₁γ₂ is predominant in the brain (Yim et al., 2017). Within the myriad of GPCR-initiated cascades, major direct targets of Gβγ are G protein-gated inwardly rectifying K⁺ channels (GIRK1-4; Kir3.1-4), voltage-gated Ca²⁺ channels (Ca_v), presynaptic SNARE proteins, some adenylyl cyclases, phospholipase Cβ, phosphoinositide 3 kinase γ, and G protein receptor kinases (Betke et al., 2012; Dascal, 2001; Sadana and Dessauer, 2009; Wickman and Clapham, 1995; Zamponi and Currie, 2013).

Among the more than 25 mutations causing *GNB1* Encephalopathy, many amino acid (a.a.) residues overlap with Gα-interacting interfaces of Gβ: a.a. 57, 78, 80, 89, 110 (Ford et al., 1998). These and additional residues in Gβ (Albsoul-Younes et al., 2001; Mirshahi et al., 2002) are also major contributors to interactions with effectors (e.g., K78 and R96 are among the key GIRK-interacting a.a. in the GIRK2/Gβγ complex (Whorton and MacKinnon, 2013)), further pointing to altered interactions of Gβ₁ with Gα or direct effectors as possible causes of the disease.

The strong neurological impact of *GNB1* mutations indicates that Gβ₁ is involved in specific aspects of neuronal signaling. A recent proteomic study identified strong link between human epilepsies and Gβ₁ protein levels in different brain regions (Pires et al., 2021). While some genetic epilepsies are caused by mutations in genes that participate in synaptogenesis, cell metabolism, cyclic AMP signaling, etc. (Mertz et al., 2020; Noebels, 2017), the major causes of epilepsy are altered neurotransmitter receptor signaling and ion channel function (Deng et al., 2014). Accordingly, when considering candidate molecular mechanisms linking *GNB1* mutations to epilepsy, we focused on GIRK and Ca_v2 channels, and the G_{i/o} proteins that are the specific source of Gβγ that regulates these channels (Dascal, 2001; Logothetis et al., 2015; Lüscher and Slesinger, 2010; Zamponi et al., 2015).

¹Department of Physiology and Pharmacology, School of Medicine, Tel Aviv University, Tel Aviv 6997801, Israel

²Department of Biotechnology, Bhupat and Jyoti Mehta School of Biosciences, Indian Institute of Technology Madras, Chennai 600036, India

³Department of Pediatrics, Schneider Children's Medical Center, Petah Tikva, Israel

⁴Departments of Psychiatry & Molecular Pharmacology and Therapeutics, Vagelos College of Physicians & Surgeons, Columbia University, New York, NY, USA

⁵Division of Molecular Therapeutics, New York State Psychiatric Institute, New York, NY, USA

⁶NNF Center for Basic Metabolic Research, Faculty of Health and Medical Sciences, University of Copenhagen, København, Denmark

⁷Institute for Genomic Medicine, Columbia University Irving Medical Center, New York, NY10032, USA

⁸Department of Genetics and Development, Columbia University Irving Medical Center, New York, NY10032, USA

⁹Sagol School of Neuroscience, Tel Aviv University, Tel Aviv, 6997801, Israel

¹⁰Present address: Dynacure, Illkirch, France

¹¹Lead contact

*Correspondence: haritha89reddy@gmail.com (H.P.R.), amal@iitm.ac.in (A.K.B.), dascaln@tauex.tau.ac.il (N.D.)

<https://doi.org/10.1016/j.isci.2021.103018>



So far, information on functional changes in neuronal molecular mechanisms caused by *GNB1* mutations has been limited. With some of the mutations, altered coupling to dopamine D1 receptor ($G\alpha_s$ -coupled) and/or reduced interaction with GRK1 (G protein receptor kinase 1) and with $G\gamma_7$ were detected by bioluminescence energy transfer (BRET) assays (Lohmann et al., 2017). Importantly, expression levels of the mutants, which may cause loss- or gain-of-function (LoF and GoF, respectively), have not been consistently tested in cellular models. We described the first mouse model of *GNB1* Encephalopathy carrying the pathogenic missense variant K78R, and showed that K78R is a GoF for GIRK channel activation and proposed that altered $G\beta_1$ signaling may cause disease in part through effects on GIRK channels (Colombo et al., 2019). No detailed mechanism was deciphered for K78R effect on GIRK channels. Here we focused on K78R and two other $G\beta_1$ mutant variants at the I80 position, I80N and I80T (the latter being prevalent among *GNB1* patients). We describe the detailed mechanism of mutation-induced changes in $G\beta\gamma$ action on physiologically relevant GIRK channels: GIRK2, GIRK1/2 and GIRK1/3 (neuronal) and GIRK4 and GIRK1/4 (cardiac).

RESULTS

Five *GNB1* mutations reveal altered $G\beta_1$ protein expression and function

The majority of known *GNB1* disease-causing germline mutations are located in exons 6 and 7 of the *GNB1* gene that encode a.a. 76 to 112 in $G\beta_1$ (Endo et al., 2020; Hemati et al., 2018; Petrovski et al., 2016). We initially examined five missense mutations from this cluster: D76G, K78R, I80T, I80N, and M101V. The K78R mutation shows gain-of-expression in *Xenopus* oocytes and, at high expression levels, K78R is a partial LoF for heterotetrameric GIRK1/2 but not for the homomeric GIRK2 channel (Colombo et al., 2019). Thus, we evaluated the expression levels and the ability of the mutant $G\beta_1$ proteins to activate the GIRK2 channels in the *Xenopus* oocyte heterologous expression system.

In the past, we often observed loss of expression for missense mutants of a variety of proteins. Therefore, we started with injecting 10 ng of mutant $G\beta_1$ RNA and 5 ng of wild-type (WT) $G\beta_1$, along with a constant dose of GIRK2 RNA (Figure 1). Surface expression levels of plasma membrane (PM)-attached $G\beta$ protein were measured in excised giant membrane patches (GMPs) (Yakubovich et al., 2015) (Figures 1A and 1B). As $G\beta\gamma$ are obligatory dimers and only dimers are transported to the PM, GMP study of $G\beta$ expression simultaneously reports the $G\gamma$ expression. Without coexpressed $G\beta\gamma$, we saw a very low fluorescent signal from the endogenous oocyte's $G\beta\gamma$ which is poorly recognized by the antibody used (Yakubovich et al., 2015). For coexpressed $G\beta\gamma$, the PM levels of I80N and I80T were similar to WT $G\beta\gamma$, whereas D76G and especially M101V showed reduced PM levels. In contrast, increased protein levels were observed for K78R, as shown previously (Colombo et al., 2019). In additional experiments, surface expression of I80N and I80T at 5 ng RNA was lower than, and with 10 ng RNA it was comparable to, the level of WT $G\beta\gamma$ achieved with 5 ng RNA (Figures 1E, S1A, and S1B).

We also measured the whole-cell GIRK currents in *Xenopus* oocytes of the same experiment as in Figures 1A and 1B (Figures 1C and 1D). At -80 mV, a switch from the physiological low- K^+ solution (LK; 2 mM K^+) to a high- K^+ (HK; 24 mM K^+) solution gives an inward current (Figure 1C, blue trace). The endogenous currents in *Xenopus* oocytes are very small under these conditions; thus, this current (I_{basal}) is mostly due to the basal activity of overexpressed GIRK channels. The net GIRK currents are obtained by subtracting the current remaining after blocking the GIRK channels by 1 mM Ba^{2+} at the end of the protocol (Rubinstein et al., 2007). Homomeric GIRK2 channels display low I_{basal} and strong activation by coexpressed WT $G\beta\gamma$ (Figure 1C, black trace) (Rubinstein et al., 2009); the basal current in cells expressing $G\beta\gamma$ is termed $I_{\beta\gamma}$. Figure 1C and 1D shows that, with these RNA doses, K78R activated GIRK2 like WT $G\beta\gamma$, whereas M101V showed small activation, which could have been caused by its low expression. I80N and I80T failed to activate GIRK2 homomeric channels despite surface expression similar to WT $G\beta\gamma$ (Figure 1C, 1D, and S1), suggesting a strong LoF toward this effector.

From here on, we focused on three disease-causing mutations: K78R, I80N, and I80T; the latter is the most common among patients (Hemati et al., 2018; Petrovski et al., 2016). K78R has been characterized in mice and partially in oocytes, but the mechanism is incompletely understood (Colombo et al., 2019). I80N and I80T are characterized here for the first time.

Molecular modeling of *GNB1* mutations effects on protein-protein interactions

Computational approaches are commonly used to predict the severity of mutations and to explore the structural basis of their effects. Unfortunately, no high-resolution structural data are available for $G\beta\gamma$

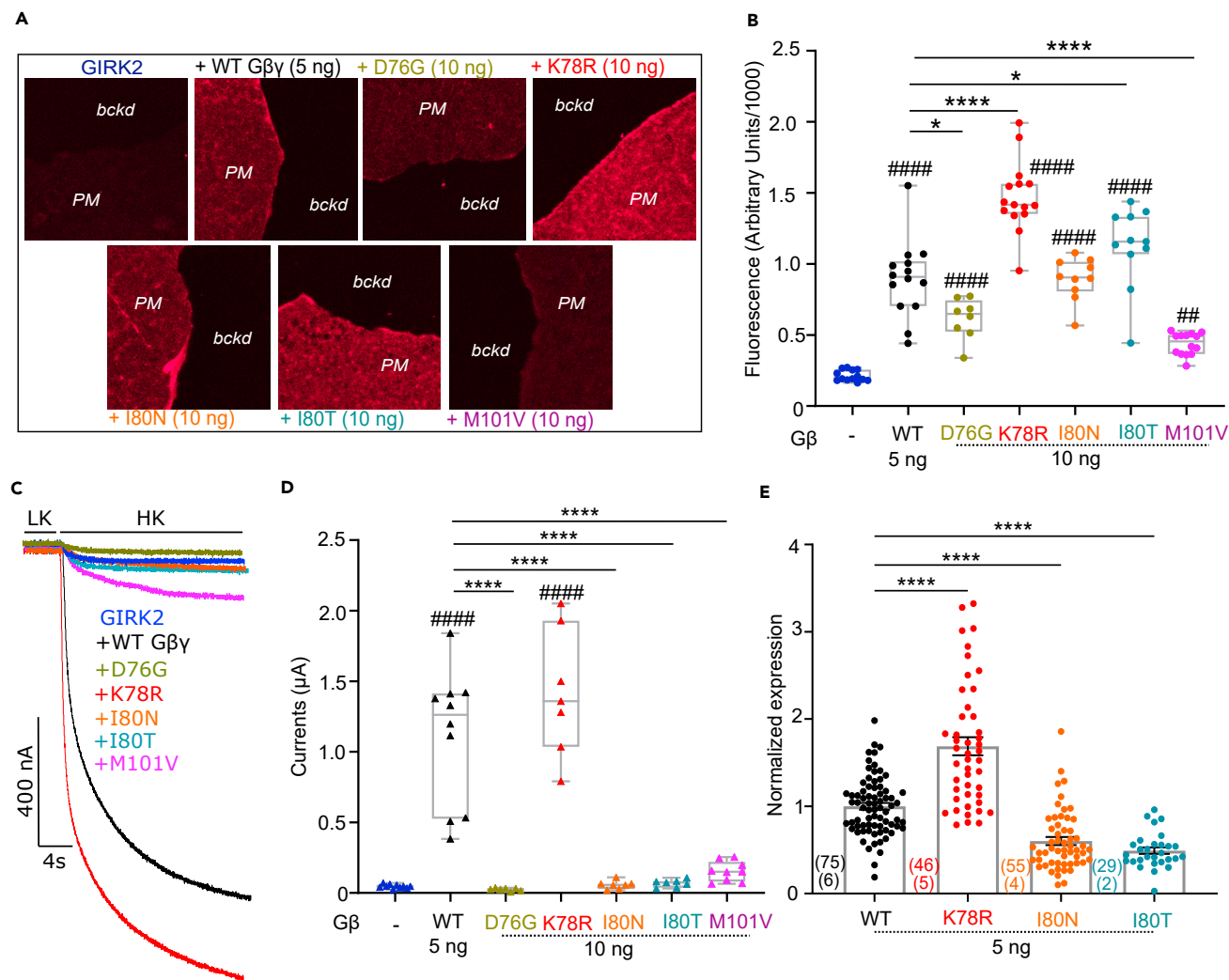


Figure 1. Initial screening of five *GNB1* mutations

Panels A-D show a single experiment.

(A) Confocal images of GMPs, stained with an antibody against Gβ, from oocytes expressing GIRK2 (RNA: 2 ng/oocyte) and Gβ WT and mutants, at indicated RNA doses. *PM*-plasma membrane, *bckd*-background.

(B) Summary of surface expression of Gβ.

(C and D) Representative current traces and (D) summary of GIRK2 currents in oocytes expressing GIRK2 alone or with WT Gβγ and Gβγ mutants.

(E) Summary of Gβγ expression, normalized to Gβγ WT, from 2 to 6 experiments with 5 ng Gβ RNA. Near the bars, number of cells (*n*; upper) and experiments (*N*; lower) are shown. Here and in the following figures, boxes (B, D) show 25th and 75th percentiles and whiskers show minimal and maximal values. Bars show mean ± SEM (E). Statistical differences are denoted as follows: asterisks (*) show comparison between WT Gβ and mutants; octothorpe sign (#) shows comparison of Gβγ-expressing groups with the channel alone (no Gβγ). * or #, *p*<0.05; ** or ##, *p*<0.01; *** or ###, *p*<0.001; **** or ####, *p*<0.0001.

interactions with Ca_v2 or SNARE proteins, and there is only one crystal structure for a “preopen” GIRK2-Gβγ complex, PDB: 4kfm (Whorton and MacKinnon, 2013). Thus, we performed a limited analysis of interaction of Gβγ with GIRK2 using 4kfm, as well as crystal structures of Gαβγ heterotrimer (Wall et al., 1995) (Figure 2A and 2B) and the Gβγ-bound G protein receptor kinase 2 (GRK2; also called β-adrenergic kinase 1, βARK1) (Lodowski et al., 2003). We also utilized two computational models for the GIRK1-Gβγ complex: the best-scoring (bs) and the largest-cluster (lc) (Mahajan et al., 2013). The analysis suggests that a.a. K78 interacts with Gα₁ (2 contacts), GIRK2 (3 contacts) and GIRK1 (2–5 contacts), whereas I80 is predicted to interact with Gα₁ (one contact) but neither with GIRK1 nor GIRK2 (Figures 2C and 2D). Next, we assessed how the mutations might affect the affinity of Gβγ interaction (reflected in ΔΔ*G*) with Gα₁, GIRK1, GIRK2, and GRK2, using the mCSM server (D. E. V Pires et al., 2014) (Figure 2E). Negative ΔΔ*G* values indicate decrease in protein-protein interaction affinity; ΔΔ*G* = −1.4 correspond to a 10 fold change (Kessel and

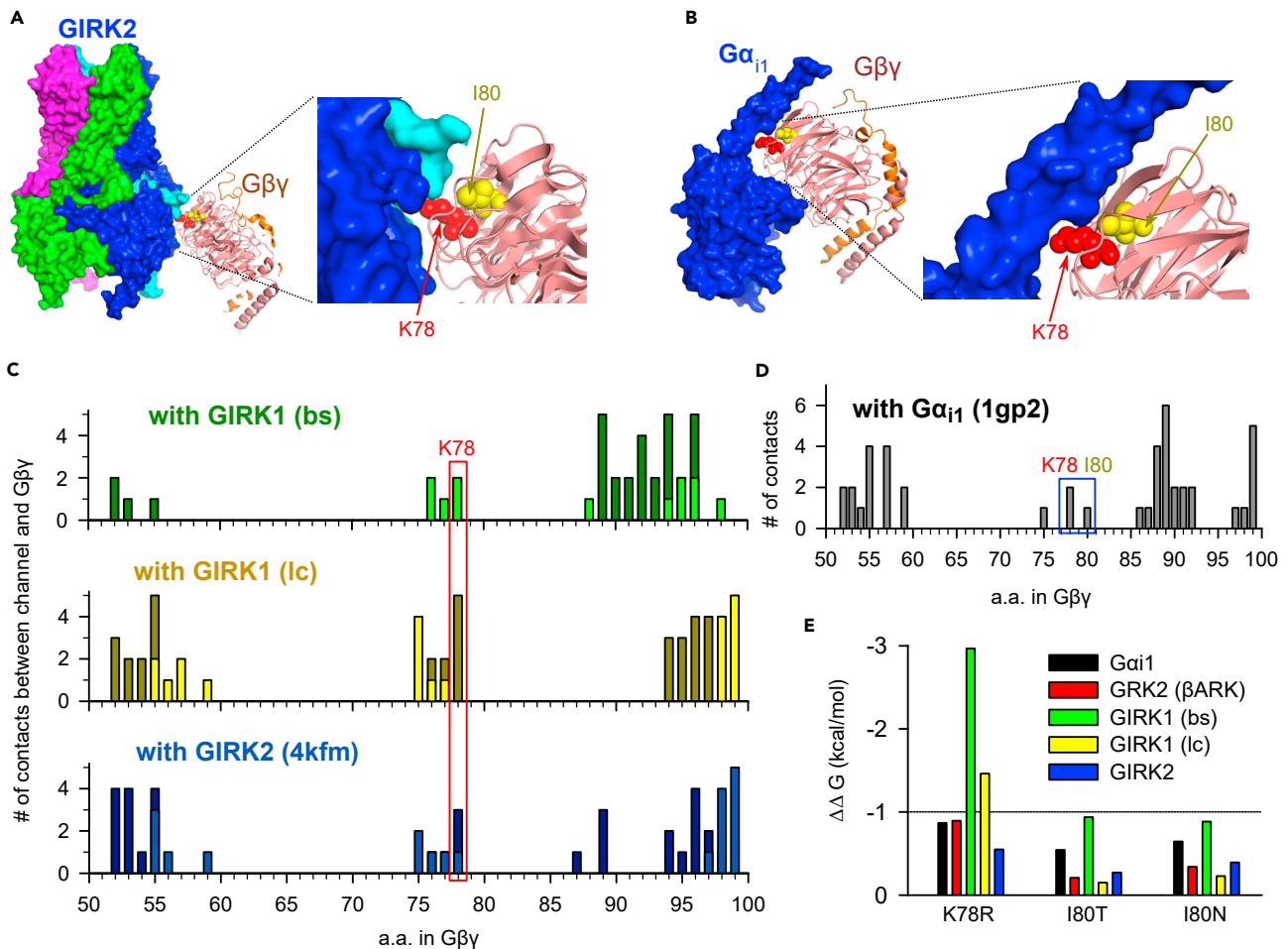


Figure 2. Structural analysis of GIRK-G $\beta\gamma$ interaction

(A) Structure of GIRK2/G $\beta\gamma$ complex (PDB: 4kfm. a.a. K78 and I80 are highlighted as red and yellow spheres; inset is zooming on the region of channel-G $\beta\gamma$ interaction.

(B) Structure of G α G $\beta\gamma$ heterotrimer (PDB: 1gp2).

(C) Analysis of a.a. contacts between G $\beta\gamma$ (a.a. 50–100) with GIRK1 (in the bs and lc models), and with GIRK2 (in the GIRK2-G $\beta\gamma$ complex). Contacts between G β with two neighboring subunits of the GIRK tetramer are shown in different shades of the same color.

(D) Analysis of interacting a.a. in G α_{i1} -G $\beta\gamma$ interface.

(E) Predicted changes of free energy of interaction of G $\beta\gamma$ with interactors following mutations of K78 and I80 in G β_1 . For GRK2-G $\beta\gamma$ complex we used PDB: 1omw. $\Delta\Delta G = -1$ kcal/mol corresponds to a ~5-fold change in affinity.

Ben-Tal, 2018). None of the mutations were predicted to significantly affect G α_{i1} -G $\beta\gamma$, GIRK2-G $\beta\gamma$, or GRK2-G $\beta\gamma$ interaction. For GIRK1-G $\beta\gamma$ interaction, K78R was the only mutant where the existing models predicted a reduction in affinity (Figure 2E).

Three GNB1 variants do not affect initial steps of GPCR signaling or G $\beta\gamma$ regulation of Ca v 2.2 channel

A potential link between a G β mutation and pathology may be a defect in the first step in G protein-mediated cascades, the activation of the G proteins by agonist-bound GPCRs. In the analysis of Figure 2, G β_1 mutations under study were not predicted to strongly affect the affinity of G $\beta\gamma$ -G α_{i1} or G $\beta\gamma$ -GRK2 interactions at rest, but did not address the dynamic changes in GPCR-G α -G $\beta\gamma$ complex caused by the agonist. We assessed the effect of mutations in G β_1 on GPCR-induced activation of G i/o proteins (which are relevant to GIRK and Ca v 2 regulation (Dascal, 2001)) using a BRET G $\beta\gamma$ release assay (Hollins et al., 2009) (Figure 3). We used dopamine D2 receptor (D2R) and split-Venus-labeled G $\beta\gamma$ (V1- γ_2 and V2- β_1) to detect the formation of G $\beta\gamma$ dimers and the dissociation of the G i/o protein complex induced by dopamine in transiently transfected HEK293T cells.

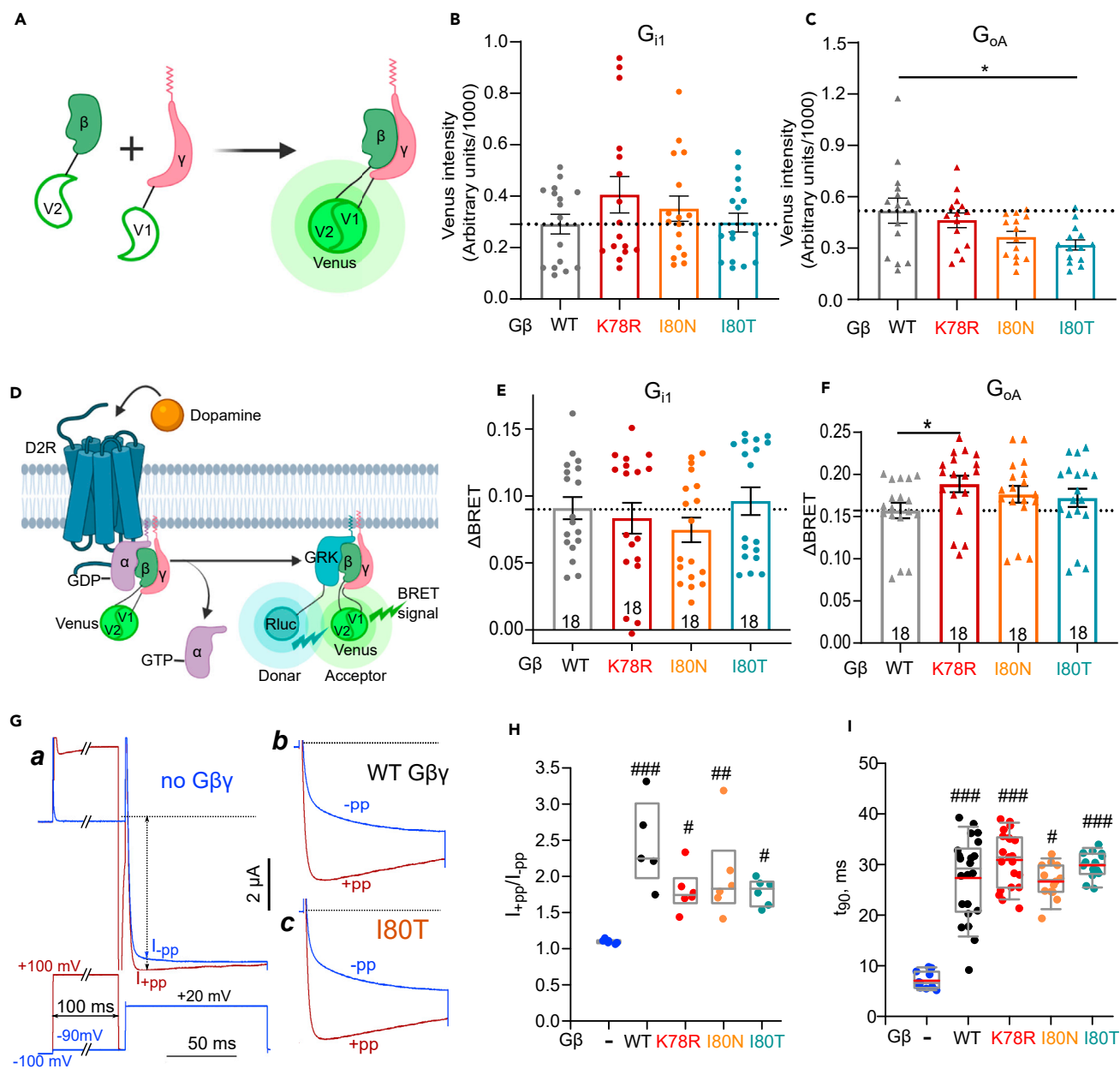


Figure 3. The three GNB1 variants do not alter Gβγ coupling to GPCR/Gα_{i/o} or Gβγ regulation of Ca_v2.2

(A) Schematic presentation of the BiFC assay to test Gβγ dimer formation. Two non-fluorescent fragments of Venus fused to Gβ (Venus 156-239-Gβ1) and Gγ (Venus 1-155-Gγ2) are brought together by interactions between Gβ and Gγ to produce a yellow fluorescent protein, Venus.

(B and C) Quantitative assessment of Gβγ dimer formation of Gβ1 mutants. Venus intensity of transiently transfected HEK293T cells to perform BRET assay was measured, and mean ± SEM from three independent experiments was plotted as a bar graph. No difference in Venus intensity between WT and mutants was observed either with Gα_{i1} (B) or Gα_{oA} (C).

(D–F) Coupling of D2R with two different Gα subunits assayed by BRET in HEK cells. (D) BRET proximity assay detects energy transfer between a donor luciferase (Rluc8) and an acceptor fluorescent protein (Venus). Rluc8 is fused to the membrane-tethered C-terminus of GRK3, GIRK3ct, which binds free but not Gα-associated Gβγ. The change in BRET signal occurs following GPCR activation, when Gβγ is released from the heterotrimeric Gαβγ and can bind GRK3. (E, F) Gβ1 mutants show no appreciable changes in agonist-induced ΔBRET, reflecting similar apparent efficiency of coupling to D2R-Gα_{i1} (E) or D2R-Gα_{oA} (F), except K78R that showed a slightly stronger ΔBRET with Gα_{oA}. Each experiment was performed 6 times with triplicate determinations.

(G) Gβγ regulation of Ca_v2.2: the experimental protocol (a, lower panel) and exemplary current traces (a, top panel, channel expressed without Gβγ; b, coexpressed with Gβγ WT, c, coexpressed with I80T). I_{ba} was evoked by a test pulse – a voltage step from –100 to +20 mV – directly without any prepulse (blue trace) or with a 100 ms-long depolarizing prepulse to +100 mV, followed by a 5 ms return to –100 mV and then the test pulse (dark red trace).

Figure 3. Continued

(H) Summary of VDF from the experiment shown in D. There was no significant difference between any of the Gβγ-expressing groups.

(I) The kinetics of activation of I_{Ba} , evaluated as t_{90} for a 50-ms depolarization, is similar with Gβγ WT and the three mutants, and is significantly slower than in control (without Gβγ). (N = 3 experiments).

First, we assessed the formation of Gβγ dimers in HEK293T cells using bimolecular fluorescence complementation (BiFC; Figure 3A) (Hu and Kerppola, 2003). All Gβ₁ mutants formed dimers with Gγ₂ similar to wild-type, evidenced by Venus fluorescence in the presence of both Gα_{i1} (Figure 3B) and Gα_{oA} (Figure 3C).

Next, we tested GPCR activation of G_{i/o}. For both Gα_{i1} (Figure 3E) and Gα_{oA} (Figure 3F), all three Gβ₁ mutants (K78R, I80N, and I80T) showed a dopamine-induced response similar to Gβ₁ WT. These results suggest that these mutations do not have a significant effect on Gα_{i/o}βγ heterotrimer association before activation by the GPCR, and the dissociation of Gβγ from Gα_{i/o} during receptor activation (see Discussion). We conclude that the above Gβ₁ mutations do not affect G_{i/o}-initiated cascades; the defect is probably further downstream, i.e., at the Gβγ-effector stage.

We next examined whether the mutations alter the inhibitory regulation by Gβγ of N-type (Ca_v2.2) voltage gated Ca²⁺ channel, a representative of the Ca_v2 subfamily (Dolphin, 2003; Tedford and Zamponi, 2006). Gβγ lowers voltage sensitivity and activation speed of Ca_v2 by shifting the gating to slowly activating ("reluctant") modes of opening (Bean, 1989). The inhibition can be relieved by strong depolarizing prepulses preceding the "test" pulse that evokes the current. We measured Ba²⁺ currents (I_{Ba}) via Ca_v2.2 in oocytes expressing the full subunit combination of Ca_v2.2 (α_{1B}, α_{2δ} and β_{2b}) with or without Gβγ (Figure 3G). We monitored the kinetic slowing of activation during a depolarizing test pulse from -90 to +20 mV, and voltage-dependent facilitation (VDF), i.e., increase in current elicited by the same test pulse after a strong depolarizing prepulse (Figure 3G). In the absence of coexpressed Gβγ, the current elicited by the test pulse without a prepulse ("I_{pp}") showed fast activation (blue trace in Figure 3Ga, top), and the depolarizing prepulse only slightly increased the current amplitude ("I_{+pp}", dark red trace). The extent of VDF, defined as I_{+pp}/I_{pp}, was 1.09 ± 0.01 (mean ± SEM, n = 6; median: 1.09; Figure 3H). This "basal" VDF may reflect the depolarization-induced relief of mild constitutive inhibition of Ca_v2.2 by an associated ambient (endogenous) Gβγ (Ikeda, 1991; Tselnicker et al., 2010). Expectedly, coexpression of WT Gβγ (Figure 3Gb) greatly slowed current activation and increased the VDF to 2.44 ± 0.24 (n = 5; median: 2.25; Figure 3H). All 3 mutations did not significantly alter the effect of Gβγ (a representative record for Gβγ I80T is shown in Figure 3Gc). The extent of facilitation was similar to WT Gβγ (Figure 3H). We also compared the kinetic slowing of the current activation, quantitated as time to 90% of current (t₉₀) reached at the end of the 100 ms depolarizing pulse in this experiment. WT Gβγ and all three mutants produced a similar kinetic slowing effect (Figure S2A). To verify this result, we pooled data from this and two additional experiments where the test pulse duration was 50 ms, having verified that t₉₀ obtained from 50 to 100 ms depolarization are linearly correlated and thus faithfully present the relative speed of current rise (Figure S2B). Figure 3I shows that WT Gβγ and all 3 mutants significantly and similarly slowed the kinetics of I_{Ba} compared to control. The depolarizing prepulse to +100 mV fully relieved the inhibitory effect of WT Gβγ and all mutants; t₉₀ (calculated from peak which usually occurred 10–15 ms after the beginning of the test pulse) was indistinguishable in control and all Gβγ groups (Figure S2C). We conclude that Gβ₁ mutations K78R, I80T and I80N do not alter the inhibitory effect of Gβγ on Ca_v2.2.

K78R, I80N and I80T affect the binding between Gβγ and cytosolic domains of GIRK1 and GIRK2 subunits

To examine whether the Gβ mutations affect the interaction between Gβγ and the GIRK subunits, we measured the direct binding of *in vitro* translated Gβγ (wt and mutants) with purified, GST-fused cytosolic domains of GIRK1 and GIRK2 (G1NC and G2NC), respectively (Figure 4). GST-G2NC comprised the full N- and C-terminal cytosolic domains connected by a 2 a.a. linker. For GST-G1NC, we initially used the protein GST-G1NC_{short} comprising a truncated cytosolic domain missing a large part of the N-terminus and the distal 130 a.a. of the C-terminus. This protein (without the GST) was previously used to determine the crystal structure of GIRK1 cytosolic domain (Nishida and MacKinnon, 2002). As shown in Figures 4A and 4C, the binding of all 3 Gβγ mutants to GST-G2NC was significantly reduced: by 25–30% for the I80T and I80N, and by ~20% for K78R. All three mutations also strongly reduced the binding of Gβγ to GST-G1NC_{short}, by ~50%. However, G1NC_{short} lacks the distal C-terminal domain, which is part of a high-affinity Gβγ binding site in GIRK1, presumably an "anchoring" site specific to GIRK1 (Dascal and Kahanovitch, 2015). To

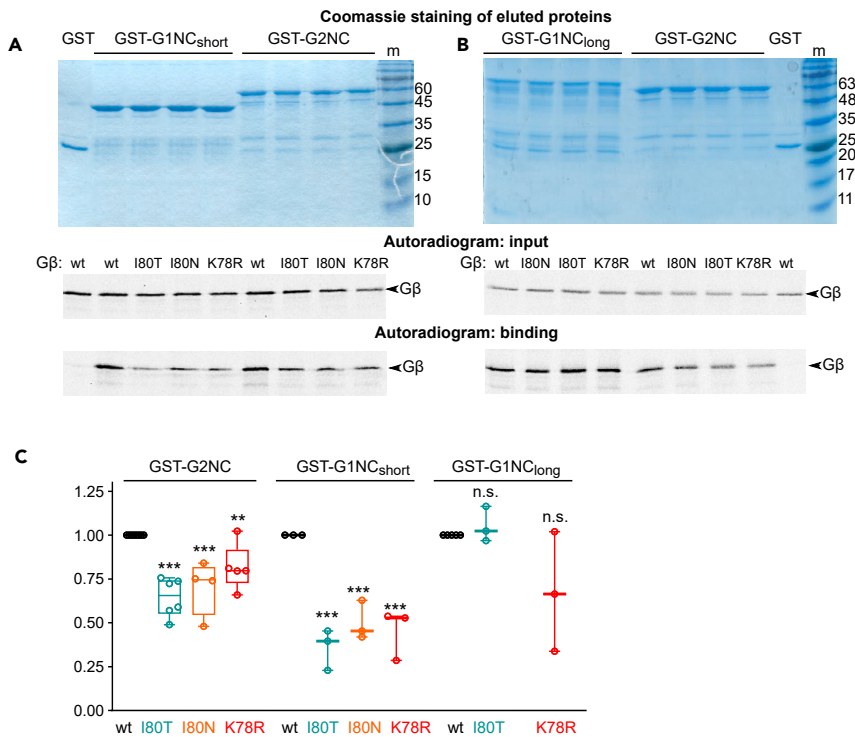


Figure 4. Effects of GNB1 mutations on the interaction between $G\beta_{1\gamma_2}$ and the cytosolic domains of GIRK1 and GIRK2

Pull-down of *invitro* $G\beta\gamma$ was done by recombinant purified GST-fused domains of GIRK2 (GST-G2NC, a.a. 1–94, 95–414) and GIRK1 (the complete cytosolic domain, G1NC_{long}, a.a. 1–84, 184–501; and the truncated construct G1NC_{short}, a.a. 41–63, 190–371) on glutathion affinity beads.

(A) Pull-down GST-G1NC_{short} and G2NC. The upper image shows Coomassie staining of the proteins bound to the beads and eluted at the end of the binding reaction. The middle panel shows the autoradiogram of the input of *invitro* proteins in reticulocyte lysate added to the binding reaction at the beginning of the incubation (1/60 of total amount), that were run on a separate gel. The lower panel is the autoradiogram of the gel shown in A (revealing the bound $G\beta$ protein).

(B) Another example of a pull-down experiment with GST-G1NC_{long} and GST-G2NC. Presentation like in A. Note that the full-length GST-G1NC_{long} protein runs in several bands on the SDS gel (Berlin et al., 2011). Of the two main bands, the upper corresponds to the full-length protein according to the calculated molecular mass.

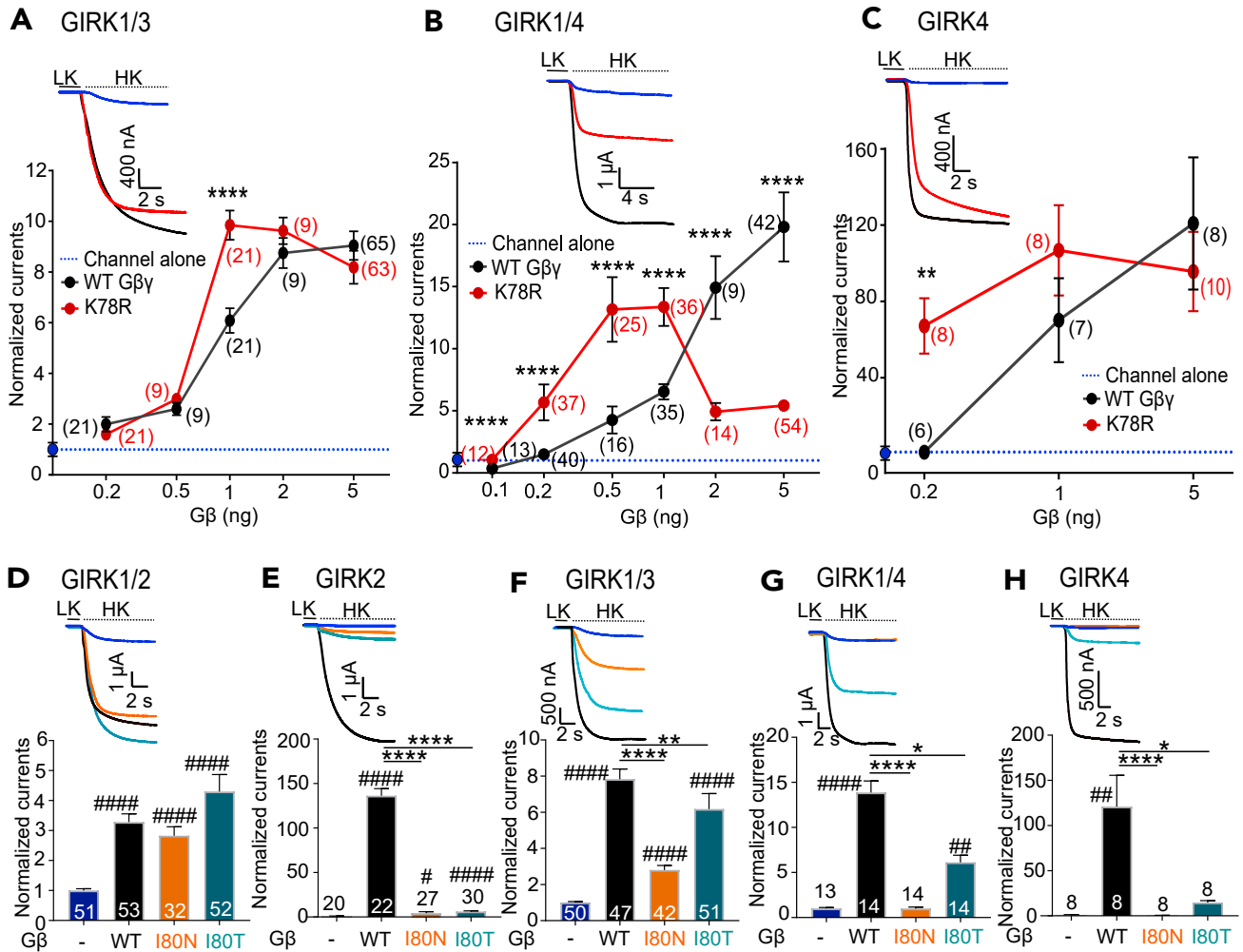
(C) Summary of the pull-down experiments. In each experiment, the binding of each construct (calculated as % of input) was normalized to that of wt $G\beta\gamma$. All data showed normal distribution and the statistical analysis was performed with one-way ANOVA followed by Holm-Sidak's multiple comparisons test. **, $p < 0.01$; ***, $p < 0.001$. All mutants show reduced binding to GST-G2NC and GST-G1NC_{short} but no significant difference in binding to G1NC_{long} (although a 30–60% reduction in binding was observed for the K78R mutants). Binding of I80N to GST-G1NC_{long} was measured only in one experiment and it was 89.6% of wt $G\beta\gamma$ (not included in the statistical analysis).

examine whether this may affect the binding of $G\beta\gamma$ mutants, we used the GST-G1NC_{long} protein that contains the complete N- and C-terminal sequences, a.a. 1–84, 184–501. This protein shows signs of partial degradation on SDS gels but binds both $G\alpha$ and $G\beta\gamma$ (Berlin et al., 2011). As seen in Figures 4B and 4C, GST-G1NC_{long} bound $G\beta_{I80T}\gamma$ similarly to wt $G\beta\gamma$, whereas the binding of $G\beta_{K78R}\gamma$ was reduced in 2 out of 3 experiments, but the difference did not reach statistical significance.

GIRKs of diverse subunit composition show differential sensitivity to $G\beta_1$ mutations

K78R has a dual effect for GIRK1/x heterotetrameric channels and GoF for GIRK homotetrameric channels

We examined the ability of $G\beta_1$ WT and K78R to activate GIRKs of physiologically relevant subunit compositions, monitored as whole-cell GIRK current, $I_{\beta\gamma}$. Initially, we used a high dose of RNA, 5ng $G\beta$ and 1ng $G\gamma$, which caused maximal activation of GIRK1/2 channels (Yakubovich et al., 2015). At this RNA dose K78R is a LoF for the heteromeric GIRK1/2 but not for the homomeric GIRK2 ((Colombo et al., 2019) and Figure 1). In



I

GNB1 mutation	Gβ1 RNA (ng)	GIRK1/2			GIRK2			GIRK1/3	
		Whole cell currents	Single channel P _o max	PM channel expression	Whole cell currents	Single channel P _o max	PM channel expression	Whole cell currents	PM channel expression
K78R (GoE mutant)	0.2	GoF	NA	NA	GoF	NA	GoE	Similar to WT	NA
	0.5	Similar to WT	Partial LoF (~66%)	Similar to WT	Similar to WT	NA	GoE	GoF	NA
	5	LoF	Partial LoF (~67%)	Partial LoE (~70%)	Similar to WT	Similar to WT	Similar to WT	Similar to WT	NA
I80N (partial LoE mutant)	5	Similar to WT	NA	Similar to WT	LoF	Severe LoF (~82%)	GoE	Partial LoF (~64%)	Similar to WT
I80T (partial LoE mutant)	5	Similar to WT	NA	Similar to WT	Severe LoF (~95%)	Partial LoF (~74%)	Similar to WT	Partial LoF (~21%)	Similar to WT

GoE- gain of expression; LoE- loss of expression; GoF- gain of function; LoF- loss of function; WT- wildtype; PM- plasma membrane; NA- not available; P_o- p open

Figure 5. Activation of different GIRK channels by G β WT vs K78R, I80N and I80T

In each experiment, current in each oocyte was normalized to the average I_{basal} of the channel-only group (dotted line in A–C). RNA doses were: GIRK1 and GIRK2 (0.05 ng each), GIRK1 and GIRK3 (3 ng each), GIRK1 and GIRK4 (1, 0.5 ng), GIRK2 (2 ng) or GIRK4 (5 ng), and the indicated amounts of G β RNA. The amount of G γ RNA was 1/5 of G β .

(A–C) Activation of GIRK1/3 (N = 1–6) (A), GIRK1/4 (N = 1–4) (B) and GIRK4 (N = 1) (C) by increasing doses of RNA of G β WT and K78R. Mann-Whitney test was done to compare WT with K78R at each RNA dose. (D–H) Effect of coexpression of G $\beta\gamma$ WT and I80 mutants (all 5 ng RNA/oocyte) on all physiologically relevant GIRK subunit compositions (N = 1–4). Number of oocytes is shown within the bars. Representative current traces with and without G β at 5 ng RNA are shown above the bar charts. I) Summary of the effects of K78R, I80N and I80T on different neuronal GIRK combinations.

contrast, at low RNA doses, K78R induced higher $I_{\beta\gamma}$ of GIRK1/2 and GIRK2 channels compared to WT G β , presumably owing to the higher expression of K78R (Colombo et al., 2019). Here, we measured the dose dependent activation of GIRK1/3, GIRK1/4 and GIRK4 by G β WT and K78R. We found that low doses of K78R yielded an apparent gain of function (GoF) effect on all channels: GIRK1/2, GIRK2 (Colombo et al., 2019), GIRK1/4, GIRK4 (Figures 5B and 5C). Interestingly, K78R had a dual effect on GIRK1/4 (Figure 5B), like on GIRK1/2: it showed an apparent GoF at low RNA doses and LoF at high doses. GIRK1/3 was an exception compared to other GIRK channels: K78R activated GIRK1/3 similarly to WT G $\beta\gamma$ at all RNA doses except for 1 ng, where a GoF was seen (Figures 5A and 5I).

I80 mutants have either partial or complete LoF effect on all GIRK channel combinations except GIRK1/2

We next studied I80N and I80T mutations, comparing G β WT and both I80 mutants in each experiment. At 5 ng G β RNA, I80 variants activated the GIRK1/2 channels similarly to WT (Figure 5D). In contrast, I80T and I80N showed LoF toward GIRK2, GIRK4, and GIRK1/4. The LoF of I80N was always more severe than of I80T (Figures 5E, 5G, 5H; summaries in Figures 5I and S3F). GIRK1/3 was partially activated by the I80 mutants (Figure 5F). We also compared G β WT vs I80N and I80T with three doses of G β RNA (0.2, 1 and 5 ng; Figure S3). I80N and I80T mutants activated GIRK1/2 channels similarly to WT at all doses except 0.2 ng (Figure S3A) but failed to activate GIRK2 (Figure S3B) and GIRK4 (Figure S3E). GIRK1/3 (Figure S3C) and GIRK1/4 (Figure S3D) were partially activated by I80 mutants. Figures 5I and S3F summarize the effects of K78R, I80N and I80T on different GIRK channel combinations.

Mutants under study are not LoF for homomeric GIRK1* channels

The above data reveal that K78R and I80T/N mutants show striking functional differences toward GIRK1-containing heterotetramers (GIRK1/2 and 1/4) vs. non-GIRK1 homotetrameric channels (GIRK2 and GIRK4). This could reflect some specific features of the GIRK1 subunit in its interaction with, or gating by, G $\beta\gamma$. GIRK1 does not form functional homotetrameric channels, but GIRK1_{F137S} mutant (GIRK1*) does, which allows to address the unique properties of GIRK1 (Chan et al., 1996; Vivaudou et al., 1997). We tested G $\beta\gamma$ RNA dose-dependent activation of GIRK1* by K78R, I80N and I80T. Interestingly, for K78R, GIRK1* was similar to GIRK2 and GIRK4 rather than to GIRK1/x channels: GoF at low RNA doses but no LoF at high doses (Figure S4A).

We verified that G γ alone (that can mildly activate GIRK1*, especially with low levels of channel expression (Tabak et al., 2019)) did not significantly activate GIRK1* in the present experiments (Figure S4B), where a relatively high dose of GIRK1* RNA was used. Thus, the LoF of K78R is only observed when GIRK1 is in combination with GIRK2 or GIRK4 (Figures 5I and S3F). In contrast, I80N and I80T activated GIRK1* similarly to G $\beta\gamma$ WT (Figures S4B and S3F).

The mechanism of LoF of G $\beta\gamma$ mutants: changes in single channel properties and channel's surface expression**K78R**

To find out why at high doses of RNA K78R has a LoF for GIRK1/2, we measured the surface expression and the single channel properties of GIRK1/2 channels. Expression of K78R caused a significant decrease in surface expression of GIRK1/2 channels compared to WT G $\beta\gamma$, to ~56% and 70% of control with 1 and 5 ng of K78R, respectively (Figures 6A and 6B; see also Figures S5D, S5E, and S5G). A plausible mechanism could be the known phenomenon of reduction of protein expression by an excess of RNA of another protein (Prelich, 2012), also observed in *Xenopus* oocytes (Oz et al., 2013), possibly due to paucity of rough endoplasmic reticulum (Richter and Smith, 1981). This reduction in GIRK level seemed to be limited to GIRK1/2 (Figure S5E) but was not specific to K78R, because a high dose of WT G $\beta\gamma$ also reduced GIRK1/2 expression, though less than K78R (Figure 6B).

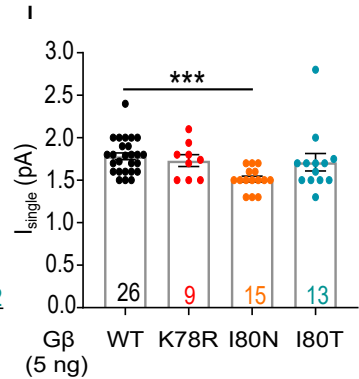
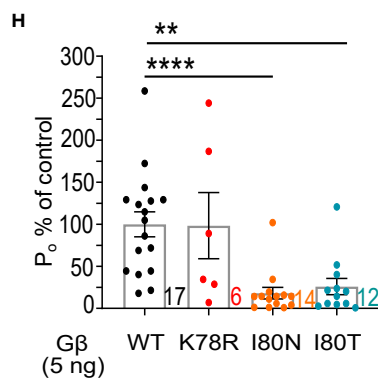
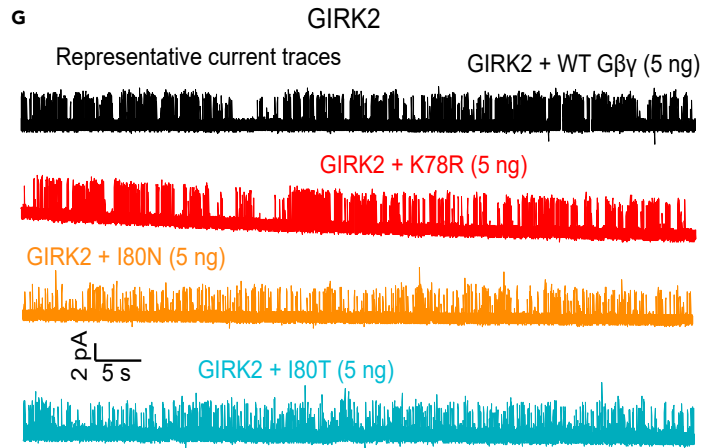
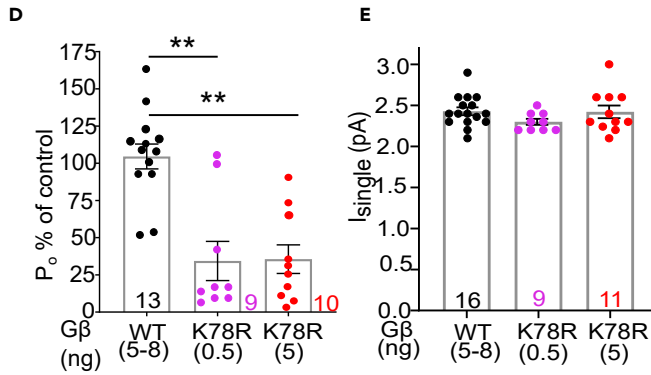
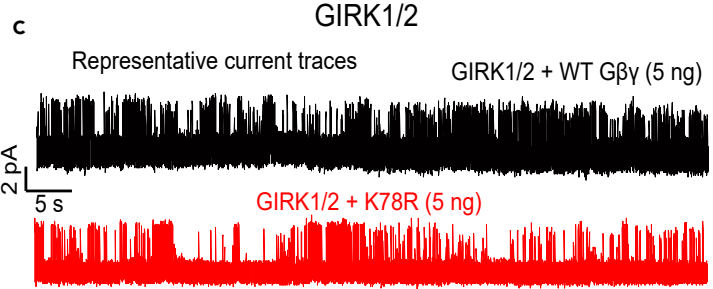
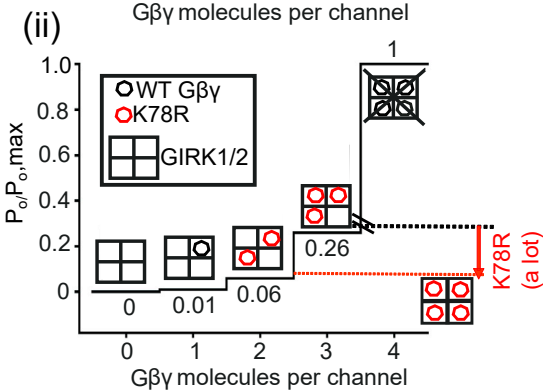
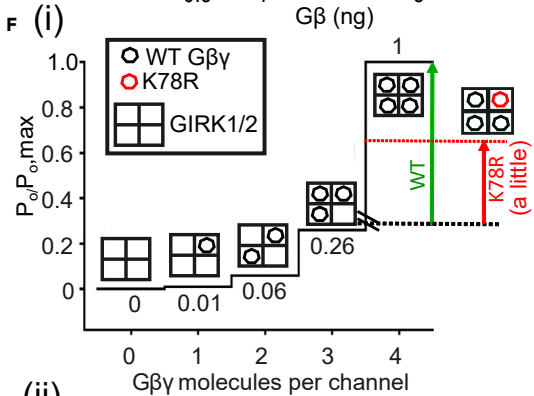
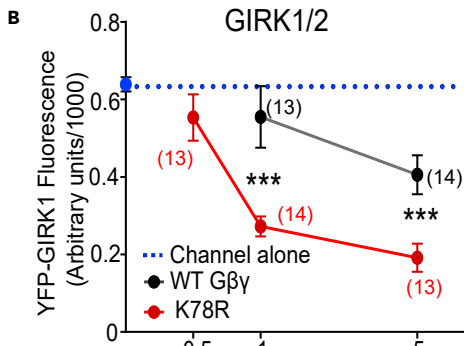
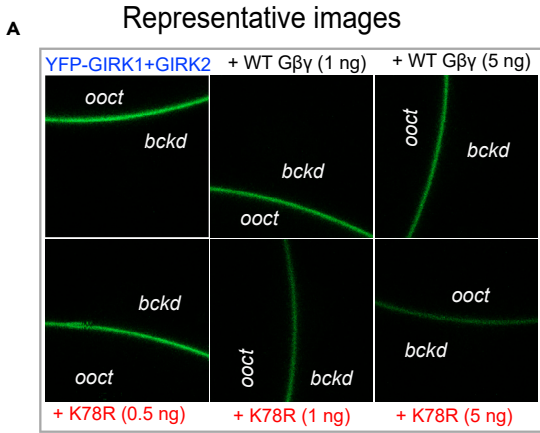


Figure 6. GIRK channel expression and single channel properties are altered in the presence of Gβ₁ mutants

RNAs doses, per oocyte, were: YFP-GIRK1 and GIRK2 (0.5 ng each), Gβ, the indicated amounts; Gγ, 1/5 of Gβ.

(A) Confocal images of oocytes expressing YFP-GIRK1/GIRK2 channels.

(B) Summary of data shown in A. Dotted line shows the surface expression level of YFP-GIRK1/GIRK2 channels without coexpressed Gβγ (N = 1).

(C) Representative cell-attached recordings of GIRK1/2 coexpressed with either Gβ WT or K78R. Upward deflections are channel openings.

(D) P_o of GIRK1/2 coexpressed with K78R or WT Gβγ, expressed as % control.

(E) i_{single} of GIRK1/2 with K78R or WT Gβγ (N = 3).

(F) A cartoon describing the explanation of the dual effect of K78R on GIRK1/2.

(G) Representative cell-attached recordings of GIRK2 coexpressed with Gβγ WT or mutants (5 ng Gβ and 1 ng Gγ RNA).

(H) P_o (% of control) of GIRK2 with WT Gβγ, I80N and I80T.

(I) i_{single} of GIRK2 is not, or only slightly (I80N), affected by the mutations (N = 3).

We also performed cell-attached single channel recordings in oocytes expressing GIRK1/2 and either Gβ WT or K78R. With Gβ WT, 5 ng RNA maximally activates GIRK1/2, thus, the open probability (P_o) measured with this RNA dose is maximal, i.e., P_{o, max} (Yakubovich et al., 2015). For K78R, maximum whole-cell GIRK1/2 currents were obtained with 0.5 ng Gβ RNA (Colombo et al., 2019). Therefore, we compared GIRK1/2 activation with 0.5 and 5 ng of K78R RNA and 5 ng of WT Gβ RNA. At both RNA doses, K78R induced a similar P_o, around 33–34% of P_{o, max} yielded by WT Gβγ (Figures 6C and 6D). The single channel amplitude, i_{single}, was identical with WT and K78R Gβγ (Figure 6E). Thus, both the reduction in P_o and in channel's surface expression leads to the LoF for GIRK1/2 observed in whole-cell recordings at high doses of K78R.

Figure 6F presents a cartoon of our hypothesis to explain the dual effect of K78R (apparent GoF at low RNA doses, LoF at high doses for GIRK1/4 and GIRK1/2), based on the graded contribution model (Yakubovich et al., 2015). GIRKs have 4 Gβγ-binding sites (Corey and Clapham, 2001; Ito et al., 1992; Whorton and MacKinnon, 2013). In GIRK1/4 and most probably GIRK1/2, each Gβγ-occupied state can contribute to GIRK1/2 channel opening and thus to P_o, with an increased extent of contribution for each additional Gβγ (Ivanova-Nikolova and Breitwieser, 1997; Sadjja et al., 2002; Yakubovich et al., 2015). The contribution of Gβγ-bound states to P_o is indicated by numbers below the "staircase" in Figure 6F (i) (0, 0.01, 0.06...). GIRK1/2 is dynamically pre-associated with 2–3 endogenous (oocyte's WT) Gβγ molecules in the basal state, which underlies its high basal activity (Yakubovich et al., 2015). At low doses of coexpressed Gβγ RNA, e.g., 0.5 ng, WT Gβγ gives very little expression and weak channel activation; but K78R Gβγ is already well expressed. Since K78R activates GIRK1/2, albeit less well than WT Gβγ, addition of one molecule of K78R Gβγ to a channel pre-associated with e.g., 3 Gβγ will confer further activation (Figure 6F (i), red arrow). At a comparable level of protein expression, WT Gβγ would have given a higher P_o (green arrow). Figure 6F (ii) analyzes the effect of high RNA doses. K78R Gβγ is overexpressed and replaces the endogenous Gβγ at most binding sites; the partial LoF nature of the K78R mutation becomes dominant and the overall P_o is decreased.

The effect of K78R on GIRK2 channel expression was also examined (Figure S5A and S5I). K78R did not alter the surface levels of GIRK2-YFP, but seemed to somewhat enhance YFP-GIRK2 levels compared to Gβγ WT, which could contribute to the GoF of K78R seen at low RNA doses. We also found no differences in single-channel parameters of GIRK2 with K78R compared to Gβγ WT (Figures 6G–6I).

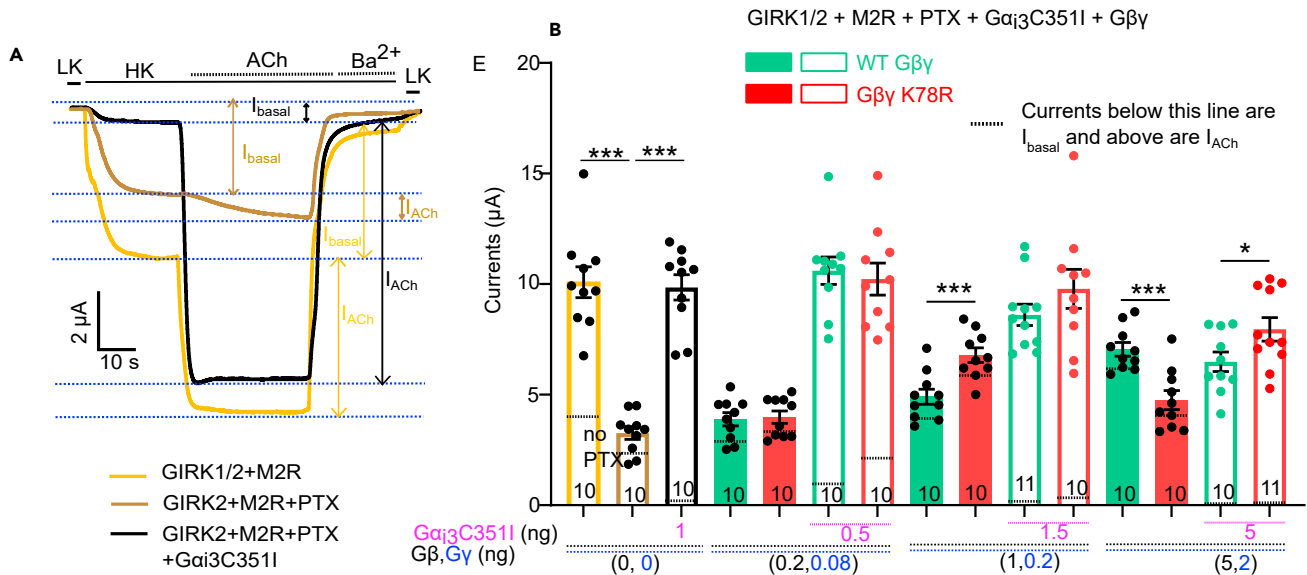
I80N/T

We observed no decrease in the surface expression of all GIRK subunit compositions coexpressed with I80N and I80T in whole oocytes, compared to WT Gβγ (Figures S5B–S5H). We also assessed the effect of coexpressed I80N and I80T on GIRK2 single channel properties (Figure 6G). Both I80 mutants failed to fully activate the channel and the P_o was drastically reduced to 18% (I80N) and 26% (I80T) compared to WT Gβγ (Figure 6H). There was no difference in i_{single} except for I80N where a small decrease was observed (Figure 6I). The latter could be a filtering artifact because of the very short duration of channel openings. The decrease in channel's open probability explains the LoF effect of I80 mutants on the GIRK2 channel.

Effects of GNB1 mutants in a fully reconstituted GPCR-Gα-Gβγ-GIRK cascade in *Xenopus* oocytes

So far we have investigated the direct activation of the GIRK channel by Gβ mutants. To address the physiological context, we reconstituted the full cascade, GPCR-Gα-Gβγ-GIRK. As a typical G_{i/o}-coupled GPCR, we used M2R (activated by 10 μM acetylcholine (ACh); Figure 7A). To inhibit the endogenous Gα_{i/o}, we expressed the A-protomer of pertussis toxin (PTX) that eliminated 80–90% of ACh-evoked current mediated

GIRK1/2



GIRK2

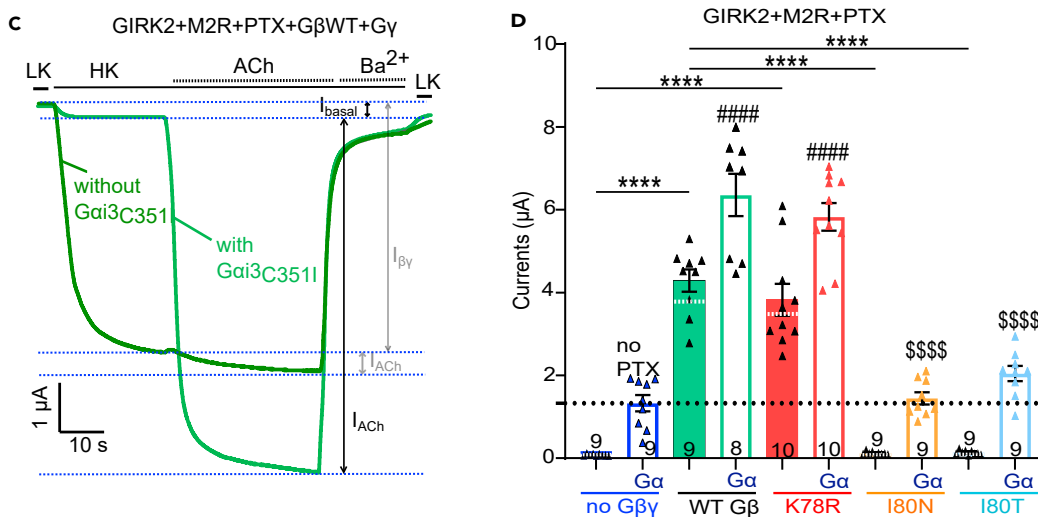


Figure 7. (A, B) Dose dependent effect of K78R on ACh activation of GIRK1/2 channels

Oocytes were injected with RNAs of GIRK1 and GIRK2 (0.1 ng), M2R (0.5 ng), without or with PTX (2 ng), and the indicated amounts of Gα₁₃C3511, Gβ and Gγ. Amounts of Gα₁₃C3511 and Gβ RNAs were increased in parallel to maintain presumably similar molar ratios optimal for the formation of Gαβγ heterotrimer. (A) Example of records where I_{basal} and I_{ACh} are shown.

(B) Summary of total currents (I_{βγ} + I_{ACh}) at -80 mV are shown. N = 1. One-way ANOVA followed by Kruskal-Wallis test; ***p<0.001. Unpaired t-test was performed to compare between WT and K78R at each Gβ RNA dose (e.g., comparison between WT and K78R at 1 ng in the presence of Gα₁₃C3511 and also comparison between WT and K78R at 1 ng in the absence of Gα₁₃C3511). ***p<0.001 and *p<0.05. Filled bars denote absence of injected Gα₁₃C3511. Empty bars denote presence of Gα₁₃C3511. Dotted black line within each bar separates basal currents from evoked currents (below the line are I_{basal} and above the line are I_{evoked}). Numbers of oocytes are shown within the bars.

(C and D) I80 mutants show LoF for GPCR-activated GIRK2 currents. Oocytes expressed GIRK2 (5 and 10 ng RNA), M2R (0.2 ng) and PTX (2 ng). In addition, Gβ (5 ng), Gγ (2 ng), and Gα₁₃C3511 ("Gα"; 2.5 ng) were expressed where indicated. (C) Example of records where I_{basal}, I_{βγ} and I_{ACh} are shown. (D) Summary of total currents ((I_{basal} + I_{ACh}) or [I_{βγ} + I_{ACh}]) at -80 mV. The black dotted line shows I_{total} of GIRK2 in oocytes expressing Gα₁₃C3511 without Gβγ. The dotted

Figure 7. Continued

white line within each shows the amplitude of I_{basal} ($I_{\beta\gamma}$). Filled bars, no coexpressed $G\alpha_{13}C3511$; empty bars, with coexpression of $G\alpha_{13}C3511$. $N = 1$ experiment; numbers of oocytes are shown within the bars. Comparison was made by one-way ANOVA followed by Dunnett's test, between no- $G\beta\gamma$ group and $G\beta\gamma$ groups either in the presence (#) or in the absence (*) of injected $G\alpha_{13}C3511$; and between $G\beta$ WT group and $G\beta$ mutant groups either in the presence (\$) or in the absence (*) of injected $G\alpha_{13}C3511$. \$\$\$\$/#####/**** $p < 0.0001$.

by endogenous $G\alpha_{i/o}$ (Berlin et al., 2011) and Figures 7A and 7B), and coexpressed PTX-insensitive $G\alpha_{13}$ ($G\alpha_{13}C3511$). However, the endogenous $G\beta\gamma$ cannot be eliminated. With 5 ng $G\beta\gamma$ RNA, a ~1.5-2-fold excess of expressed $G\beta\gamma$ over endogenous $G\beta\gamma$ is expected (Yakubovich et al., 2015), but part of the GPCR-induced response will unavoidably be mediated by the endogenous $G\beta$ (somewhat like in a heterozygotic condition, as in GNB1 encephalopathy patients). RNA titration of $G\alpha_{13}C3511$ in the presence of $G\beta\gamma$ and coexpressed $G\beta\gamma$ WT, using GIRK1/2 as readout (Figure S6A) showed that overwhelming excess (~5 fold) of $G\alpha_{13}C3511$ RNA over $G\beta$ yields greatly reduced total current, reflecting a $G\beta\gamma$ -scavenging effect of excess $G\alpha$ (Rubinstein et al., 2007); ~2.5 fold $G\alpha$ excess over $G\beta$ yielded an optimal situation with low basal current (I_{basal}) and a robust ACh-evoked current, I_{evoked} (or I_{ACh}), whereas the total current (I_{total}), which is the sum of I_{basal} and I_{ACh} , was not reduced (Figures 7B and 7D; S6A–S6C). In the following experiments we adjusted the amounts of $G\beta$ and $G\alpha_{13}C3511$ RNA to obtain similar near-optimal conditions.

K78R has GoF effect but not a dual effect on GIRK1/2 channels when activated through M2R

We examined M2R/ $G\alpha_{13}C3511$ -mediated activation of GIRK1/2 channels with three RNA doses of $G\beta$ WT or $G\beta$ K78R (Figure 7B). For each $G\beta\gamma$ dose, the RNA dose of $G\alpha_{13}C3511$ was adjusted to obtain low I_{basal} but avoiding the scavenging effect. The three leftmost bars of Figure 7B summarizes the effect of PTX and $G\alpha_{13}C3511$ on GIRK1/2 in the absence of $G\beta\gamma$, confirming the elimination of I_{ACh} mediated by endogenous $G\alpha_{i/o}$ and demonstrating restoration of I_{ACh} by coexpression of $G\alpha_{13}C3511$. K78R showed the expected GoF 1.5 ng and LoF at 5 ng RNA in the absence of coexpressed $G\alpha_{13}C3511$ (compare filled green bars and filled red bars in Figure 7B). However, total currents in the presence of $G\alpha_{13}C3511$ indicated a possible GoF effect of K78R on GIRK1/2 at 1 ng and 5 ng doses but reached significance only at 5 ng doses.

I80N and I80T are LoF mutants for GIRK2 channels

We activated the GIRK2 channels by M2R via $G\alpha_{13}C3511$ and $G\beta\gamma$ (WT or I80T/N). WT $G\beta\gamma$ was at 5 ng $G\beta$ RNA, I80N/T at 5 ng (Figure 7D) or 10 ng $G\beta$ RNA (Figure S6B) to assure similar expression levels to WT $G\beta$ (see Figures 1B and S1B). Both I_{total} and I_{ACh} were greatly reduced with I80N and I80T compared to $G\beta$ WT, confirming LoF that we saw with direct GIRK2 activation by coexpressed $G\beta\gamma$. The remaining I_{ACh} is comparable to that in control without coexpressed $G\beta\gamma$ (empty black bar in Figure 7D), and thus may result from endogenous $G\beta\gamma$ associated with $G\alpha_{13}C3511$ and then released after the activation of M2R. However, there also may be a contribution from the I80 mutants, which can produce weak activation of GIRK2 (see Figures 5E and S3B). We also observed good GPCR-induced activation of GIRK2 with K78R (Figure 7D), and of GIRK1/2 with I80N/T (Figure S6C), similar to activation seen with WT $G\beta$. This confirms that K78R activates GIRK2 and I80 mutants activate GIRK1/2 such as WT $G\beta\gamma$, and strongly supports the notion that GPCR- $G\alpha_{i/o}$ part of the cascade is not impaired by these mutations.

GIRK channel openers VU0529331 and ML297 can rescue channel activity

The LoF effect of I80 mutants on $G\beta\gamma$ activation of GIRK1/3 and GIRK2 channels may potentially contribute to disease symptoms, and increasing the activity of channels by $G\beta\gamma$ -independent openers may prove beneficial. We used VU0529331 (VU; non-GIRK1 channel opener) (Kozek et al., 2019) to rescue GIRK2 activity and ML297 (GIRK1/X channel opener) (Kaufmann et al., 2013) to rescue GIRK1/3 channel activity in the presence of coexpressed I80 mutants.

VU0529331(VU) rescues GIRK2 channel activity in the presence of I80N/T mutants

Cells were first exposed to the high-K solution to measure I_{basal} or $I_{\beta\gamma}$, and then VU was added at 2.5, 10, or 40 μM . VU activated GIRK2 (Figures 8A–8D), alone or with coexpressed $G\beta\gamma$. Currents measured in each oocyte before and after the application of VU are shown in Figures S7A–S7D. VU induced a strong activation of the channel expressed without $G\beta\gamma$ (~100-fold) or with I80T/N (10–20 fold) (Figure 8D). K78R alone yielded GIRK2 currents greater than with the WT $G\beta\gamma$ (Figure 8B), and 40 μM VU induced only a slight further increase (Figures 8C and 8D). Interestingly, regardless of the initial current amplitudes in each group under study (Figure 8B), with 40 μM VU similar GIRK2 amplitudes were achieved (10–16 μA ; Figure 8C).

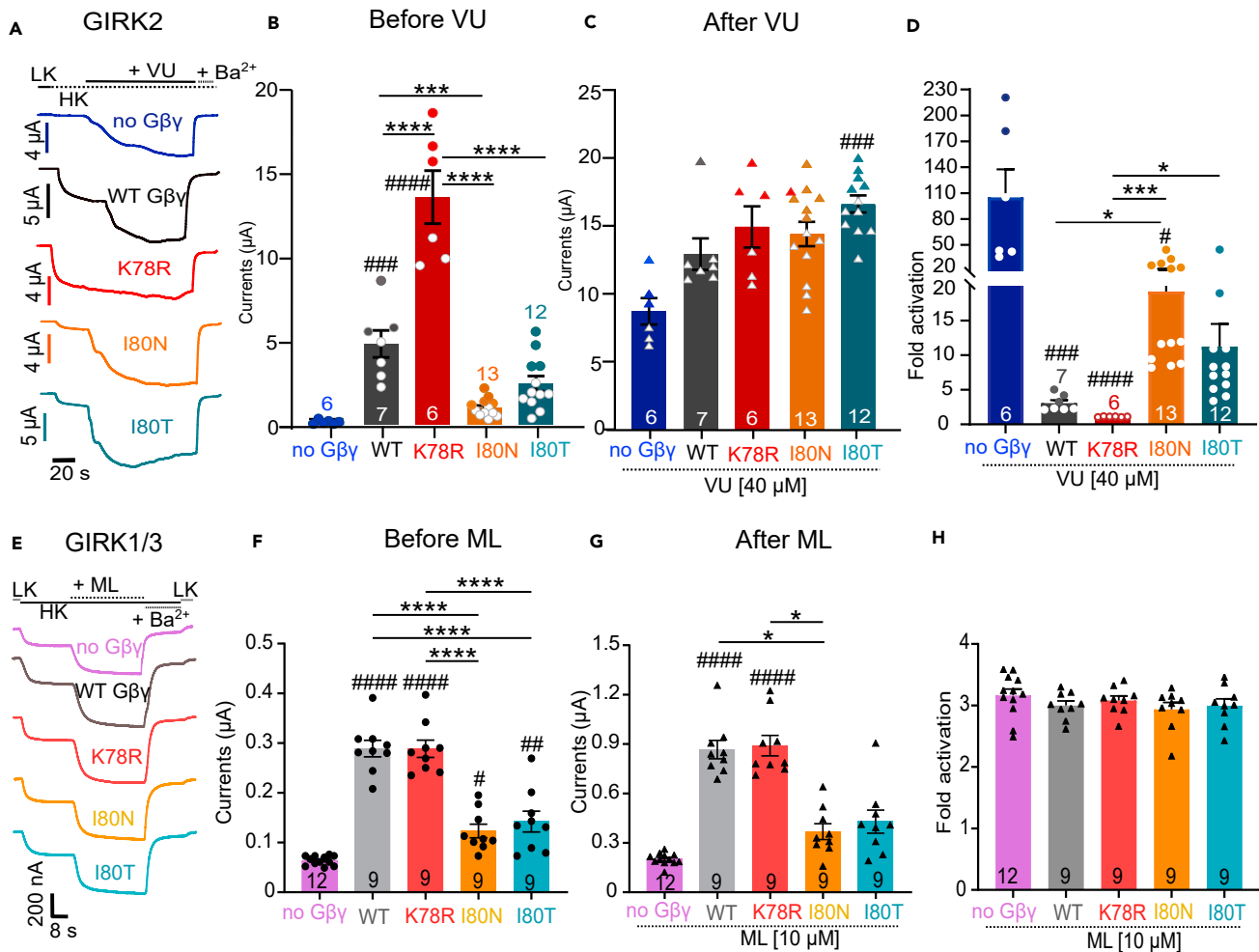


Figure 8. Rescue of GIRK channel activity by VU0529331 and ML297 in the presence of LoF mutants I80N and I80T
Oocytes expressed GIRK2 (2 ng RNA) or GIRK1/3 (3 ng) channels, with or without Gβ WT (5 ng), I80N and I80T (10 ng), and Gγ (1/5 of Gβ).
(A) Representative records of GIRK2 currents and their activation by 40 µM of VU0529331 in oocytes expressing Gβγ.
(B and C) Summary of GIRK2 currents with and without Gβγ before (B) and after (C) the application of 40 µM VU0529331.
(D) Fold activation of GIRK2 by 40 µM of VU0529331.
(E) GIRK1/3 currents and their activation by 10 µM of ML297 in the presence of Gβγ.
(F and G) Summary of GIRK1/3 currents with and without Gβγ before (F) and after (G) the application of 10 µM ML297.
(H) Fold activation of GIRK1/3 by 10 µM of ML297 (N = 1).

Thus, VU, which is known to activate GIRK2 channel in a Gβγ-independent manner (Kozek et al., 2019), apparently activates all the channels to the fullest with or without Gβγ.

ML297 partially rescues GIRK1/3 channel activity in the presence of I80N/T mutants

ML297 was initially tested at three doses (2.5, 10 and 40 µM). Representative current traces are shown in Figure 8E. Currents before the application of ML297 are shown in Figure 8F. We observed maximum activation at 10 µM, and 40 µM activated similarly or even less efficiently in some of the groups (Figures S7F–S7J). With 10 µM ML297, activation was approximately 3-fold, irrespective of the presence or absence of Gβγ (Figures 8G and 8H).

DISCUSSION

GNB1 mutations cause epilepsy; altered Gβ₁ protein levels are associated with human epilepsies (Pires et al., 2021). Revealing the specific neuronal mechanisms underlying the links between Gβ₁ and epilepsy

can spur development of treatments using precision personalized medicine (Noebels, 2017; Torkamani et al., 2017). Initial screening of five $G\beta_1$ mutants in *Xenopus* oocytes (Figure 1) indicated that all mutations affected surface expression levels of $G\beta_1$ protein, despite equal amounts of RNA injected. Such changes could be potentially important in disease etiology. We further performed a computational and functional study of three mutations (K78R, I80N, and I80T), focusing on three plausible pathways that may link $G\beta_1$ to epilepsy: coupling to GPCR and $G\alpha_{i/o}$, and regulation of two ion channels, GIRKs and $Ca_v2.2$, which are classical effectors of $G\beta\gamma$. Only GIRK channels were affected by the $G\beta_1$ mutations under study. We report highly specific effects of $G\beta_1$ mutations on regulation of GIRK channels, address and resolve the cellular and biophysical mechanisms of mutations' effects on $G\beta\gamma$ regulation of main neuronal GIRKs (GIRK1/2, GIRK2, and GIRK1/3), and demonstrate full or partial rescue of LoF of I80N/T mutations toward GIRK2 and GIRK1/3 by GIRK openers. Our findings help to better understand the etiology of GNB1 encephalopathy and yield new insights into general mechanisms of $G\beta\gamma$ regulation of GIRKs.

Focus on GIRKs

We determined that K78R and I80N/T mutations of $G\beta_1$ do not affect the coupling between GPCRs and $G_{i/o}$ proteins or the association/dissociation of $G\beta\gamma$ with $G\alpha_{i/o}$ before/after receptor activation. This is supported by three lines of evidence. First, an analysis of structural models predicted unimpaired $G\alpha_{i/o}$ - $G\beta\gamma$ interactions (Figure 2). Second, the BiFC assay showed proper formation of $G\beta\gamma$ complexes, suggesting intact $G\beta$ - $G\gamma$ interaction (Figures 3A–3C). The functional BRET assay (Figures 3D–3F) demonstrated a similar regulation of the $G_{i/o}$ proteins by a GPCR (D2R) with $G\beta_1$ mutants and WT $G\beta_1$. These results suggest a proper dissociation of $G\beta\gamma$ from $G\alpha$ and intact binding of free $G\beta\gamma$ to the reporter, GRK3. Moreover, the results also indicate an intact association of $G\beta\gamma$ with $G\alpha$ before GPCR activation; otherwise, the dissociation would have been hindered (although modest changes in $G\alpha$ - $G\beta\gamma$ affinity might not be detected). Third, GPCR-induced activation was unimpaired for channel/ $G\beta_1$ mutant pairs (GIRK1/2 by I80T/N, (Figure S6C) and GIRK2 by K78R (Figure 7D)) that also showed normal activation in a direct $G\beta\gamma$ activation assay (i.e., by $G\beta\gamma$ coexpression).

Functional oocyte experiments also did not reveal any changes in $G\beta\gamma$ regulation of $Ca_v2.2$, a representative of the Ca_v2 voltage-gated Ca^{2+} channel class (Figures 3G–3I). Given these results, the strong LoF in $G\beta\gamma$ regulation of GIRK2 by I80N/T (Figure 1), the decrease in $G\beta\gamma$ -GIRK interaction for all 3 mutants observed in direct binding experiments (Figure 4), and the previous indications of the involvement of GIRKs in K78R-induced epileptic symptoms in mice (Colombo et al., 2019), we further focused on GIRKs. We have distinguished between effects of changes in protein expression from alterations in $G\beta\gamma$ -GIRK coupling by concomitantly monitoring whole-cell currents and the surface levels of both GIRK and $G\beta\gamma$ proteins. We compared all GIRK1/x heterotetramers with the homomers—GIRK2, GIRK4, and GIRK1* (GIRK1* is the GIRK1_{F137S} mutant that yields functional homotetrameric channels). For GIRK1/2 and GIRK2 we also analyzed single channel parameters, which report the functional changes in $G\beta\gamma$ activation of GIRKs on a single-molecule level. A central finding was that $G\beta_1$ mutations cause profound changes in GIRK regulation, which are divergent and mutation- and channel composition-specific (see Figures 5I and S3F for a summary).

$G\beta_1$ mutations reduce $G\beta\gamma$ interaction with GIRK1 and GIRK2 cytosolic domains

Assaying $G\beta\gamma$ -GIRK interaction by pulldown (Figure 4) directly reports changes in protein binding, but there are limitations. First, the truncated GIRK1 cytosolic domain (G1NC_{short}) folds correctly and tetramerizes in solution (Nishida and MacKinnon, 2002; Yokogawa et al., 2011), but it is not known if this is also true for the GST-fused full-length cytosolic domains of GIRK2 (G2NC) and GIRK1 (G1NC_{long}). Second, absence of the transmembrane domain may undermine the cooperativity of $G\beta\gamma$ binding, in effect reducing $G\beta\gamma$ -GIRK affinity (Wang et al., 2016). These reservations notwithstanding, the direct binding results are in line with the observed functional changes in GIRK2 channel regulation (see Figure 5I), showing a 25–30% decrease in binding of I80 mutants to G2NC and a ~20% decrease for K78R (Figure 4). G1NC_{long} bound I80T like the WT $G\beta\gamma$, whereas a marginal decrease was observed for K78R. This is also in general agreement with functional data, where all mutants well activated the GIRK1* homotetramer (Figure S4). Interestingly, for G1NC_{short}, all three $G\beta\gamma$ mutants showed ~50% reduction in binding. We hypothesize that the $G\beta_1$ mutations under study reduce the $G\beta\gamma$ binding to main $G\beta\gamma$ “activation” site located in the core of GIRK1 cytosolic domain (Dascal and Kahanovitch, 2015), but are less detrimental for $G\beta\gamma$ binding to the high-affinity “anchoring” site, that includes the distal C-terminus of GIRK1 present in G1NC_{long} but missing in G1NC_{short} (Kahanovitch et al., 2014).

The complex effects of the K78R mutation

Of the three $G\beta_1$ mutants, K78R showed the most complex pattern of effects. Surface protein expression of K78R was consistently higher than WT $G\beta\gamma$, with equal amounts of RNA introduced into oocyte (“gain of expression”), especially at low RNA doses (Colombo et al., 2019, and Figure 1). However, the functional effect of K78R, namely on total (whole-cell) GIRK currents, differed depending on $G\beta$ RNA dose and channel composition.

At low RNA doses K78R showed GoF: it increased whole-cell currents of all GIRK compositions, without altering channels’ surface expression (Figures 6 and S5). However, K78R never increased the P_o or the single channel current of GIRK2 or GIRK1/2. These results strongly suggest that the GoF (increase of whole-cell GIRK activity) of all GIRK compositions at low K78R RNA doses was mainly due to gain of expression of the $G\beta_{K78R\gamma}$ protein. The gain-of-expression, together with a modest enhancement of GIRK2 protein in the PM (Figures S5A and S5I) can probably compensate for the minor loss of binding to GIRK2 (Figure 4).

At high RNA doses, K78R still showed somewhat higher protein expression than the WT $G\beta\gamma$ but yielded similar activation of homomeric GIRK2 and GIRK4 on the whole-cell level, possibly due to a “ceiling” effect, e.g., by reaching a maximal P_o (Figures 1 and 5 and (Colombo et al., 2019)), and/or owing to a modest reduction in binding to GIRK2 (Figure 4). In contrast, in GIRK1/2 and GIRK1/4 K78R showed a clear LoF manifested in a strong reduction in whole-cell current, compared to WT $G\beta\gamma$ or to low RNA doses of K78R. We discovered that this was due to the combined effect of reduced P_o and reduced GIRK1/2 channel expression in whole oocyte. Overall, our data provide a satisfactory mechanistic explanation for the dual, RNA dose-dependent effect of K78R on $G\beta\gamma$ regulation of GIRK1/2 (Figure 6F), and probably the homologous GIRK1/4, with gain-of-expression being dominant at low and LoF at high RNA doses. Interestingly, GIRK1/3 stood alone among the GIRK1/x heterotetramers, showing little sensitivity to the K78R mutation in $G\beta_1$ (Figure 5), suggesting specific channel properties conferred by the least homologous GIRK3 subunit.

Overall, we posit that due to its gain-of-expression, K78R would be acting as GoF for GIRKs under physiological conditions when no great excess of $G\beta\gamma$ is expected. This is supported by two lines of evidence. First, in reconstituted full GPCR (M2R) -GIRK1/2 cascade (Figure 7), a GoF effect of K78R was observed with intermediate and high doses of K78R RNA (Figure 7B), indicating the possible involvement of endogenous $G\beta\gamma$ that blunts some of the difference at low K78R RNA doses. We have not detected any LoF in the range of $G\beta\gamma$ expression levels tested. Second, the hyperexcitability in cultured neuronal networks and the epilepsy in the genetically engineered (GE) $Gnb1^{K78R/+}$ (K78R/+) mouse were corrected by ethosuximide (Colombo et al., 2019), an antiepileptic drug that is a potent GIRK blocker (Colombo et al., 2019; Kobayashi et al., 2009), though originally described as a blocker of T-type Ca^{2+} channels (Gomora et al., 2001). Hyperexcitability associated with excessive activity of a K^+ channel is counterintuitive but may occur in neuronal networks if, for example, this activity takes place mainly in inhibitory interneurons (Shore et al., 2020).

I80N and I80T are mostly LoF

Both I80 mutants are full or partial LoF for most GIRK channel compositions but, quite strikingly, not for GIRK1/2 channels. In addition, I80 mutants showed a partial loss of expression, which we compensated by doubling the RNA amounts of I80N/T (Figures 1 and S1). Both I80N and I80T failed to activate GIRK2 channels, either direct activation by over expressed $G\beta\gamma$, or $G\beta\gamma$ release following activation of a GPCR (Figures 1, 5, 7, and S6). GIRK2 channels coexpressed with I80N or I80T showed a greatly reduced P_o . At the same time, GIRK1/2 channels were activated by I80N and I80T like the WT $G\beta\gamma$, corroborating the proper surface expression and functionality of I80N/T. Thus, I80N/T mutants are genuine LoF mutations. We note that the changes in $G\beta\gamma$ binding to full-length GIRK2 cytosolic domain were rather mild, suggesting that part of the observed LoF could be also due to deficiencies in gating (the $G\beta\gamma$ -induced conformational changes in the channel protein that lead to channel opening).

The decrease in GIRK2- $G\beta\gamma$ binding and LoF of the I80T/N mutants toward GIRK2 suggests the importance of the I80 a.a. residue in $G\beta_1$ -GIRK2 interaction. However, no such interaction is present in the only available crystal structure of the GIRK2- $G\beta\gamma$ complex (Whorton and MacKinnon, 2013), indicating the existence of additional interaction conformations, a perturbation in $G\beta\gamma$ -GIRK interface indirectly caused by this mutation, or an allosteric effect.

Gβ mutations offer insights into structural details of Gβγ-GIRK interactions

The differential effects of the Gβ₁ mutations on homo- vs. heterotetrameric GIRKs point to potential structural differences. For K78R, we saw LoF for GIRK1/2 but not for GIRK2 (for equal Gβγ protein levels). Interestingly, K78R also does not show LoF with the homotetrameric GIRK1*, regulating it like GIRK2 (Figure S4): apparent GoF at low RNA doses of K78R (probably due to gain-of-expression), but no LoF at high doses of K78R. Also, Gβ_{K78R}γ binds to the full cytosolic domain of GIRK1 only slightly less than WT Gβγ (Figure 4). LoF is only observed when GIRK1 is in combination with GIRK2, suggesting specific modes of interaction of Gβγ with heterotetrameric vs. homotetrameric GIRKs. The results with I80T/N support this notion. I80N and I80T were LoF for GIRK2 and GIRK4, but fully activated the GIRK1* homotetramer. These results imply a normal interaction with GIRK1 but an impaired one with GIRK2, as also supported by data of Figure 4 (compare I80T binding to full-length GIRK2 and GIRK1 cytosolic domains). One would then expect a partial LoF for I80I/T toward heterotetrameric GIRK1/x. Accordingly, a partial LoF was observed for I80N/T mutants with GIRK1/4 and GIRK1/3. However, no LoF was seen with GIRK1/2, despite the importance of GIRK2 for GIRK1/2 activation (Guo et al., 2002; Stevens et al., 1997). Gβγ binds to the interface of two GIRK subunits (Mahajan et al., 2013; Whorton and MacKinnon, 2013; Yokogawa et al., 2011). Therefore, we hypothesize that the distinct effects of Gβ mutations on GIRK heterotetramers may be due to a variable involvement of individual a.a. within the diverse interaction interfaces.

An additional interesting insight is provided by the effect of VU0529331 (VU), a specific Gβγ-independent opener of non-GIRK1 channels (Kozek et al., 2019), which we used to rescue GIRK2 channel activity for I80N/T mutants (Figures 8 and S7). VU potentiated the whole-cell GIRK2 currents that reached similar maximum amplitudes, regardless of the presence of Gβγ and the mutation in Gβ₁. The extent of activation by VU was highest for non-activated channels and smallest for channels coexpressed with Gβγ variants (WT and K78R) that strongly activated GIRK2. This phenomenon may indicate a common final conformational step(s) leading to the opening of GIRK2, onto which both Gβγ and VU activation converge, which deserves further study. In comparison, ML297, a Gβγ-independent specific opener of GIRK1/x channels (Kaufmann et al., 2013; Wydeven et al., 2014), showed a different pattern in activating GIRK1/3. Regardless of the functionality of Gβ (the fully functional WT and K78R, or the LoF I80T/N), the activation of GIRK1/3 by ML297 was always ~3 fold in all cases.

Our study highlights the GIRK channels as potentially important players in *GNB1* Encephalopathy. Previous studies demonstrated strong links between malfunction or altered expression of neuronal GIRKs and epilepsy (Jeremic et al., 2021; Luján et al., 2014; Lüscher and Slesinger, 2010) and GIRK openers have been found beneficial in treating several types of epilepsy in animal models (Huang et al., 2018; Weaver and Denton, 2021; Wydeven et al., 2014; Zhao et al., 2020). Accordingly, the use of GIRK-directed therapies should be considered for treating the epileptic symptoms in *GNB1* Encephalopathy. Notably, we find that each *GNB1* mutation is unique and has different effects (GoF/LoF/dual) on different GIRK channel combinations. Knowing the exact mechanism of a particular mutation will be crucial for setting the correct course of personalized treatment. In the *Gnb1*^{K78R/+} knock-in mouse, the epileptic activity was reversed by GIRK-blocking ethosuximide (Colombo et al., 2019), in line with the GoF property of K78R. In contrast, patients with LoF mutation (I80N/T) may benefit from GIRK openers, such as VU0529331 to activate GIRK2 and ML297 to activate GIRK1/3.

Limitations of the study

We addressed the molecular mechanisms of changes in Gβγ function caused by three *GNB1* mutations, that could lead to changes in neuronal excitability and epilepsy, focusing on potential defects in GPCR-G_{o/i} initiated cascades that regulate ion channels. We identified GIRKs as potential key players strongly affected by the mutations, whereas the GPCR-G_{v/o} coupling and the function of Ca_v2.2 channels was intact. However, we cannot rule out mutation-induced changes in Gβγ regulation of the other two members of the Ca_v2 class (Tedford and Zamponi, 2006), or other Gβγ-modulated ion channels. Also, we have not studied Gα_s- or Gα_q-coupled GPCR signaling and do not know if it is affected by *GNB1* mutations. Somatic mutations in *GNB1* induce carcinogenesis, possibly affecting multiple signaling pathways (Yoda et al., 2015; Zimmernannova et al., 2017) that might be linked to epilepsy.

STAR★METHODS

Detailed methods are provided in the online version of this paper and include the following:

- **KEY RESOURCES TABLE**
- **RESOURCE AVAILABILITY**
 - Lead contact
 - Materials availability
 - Data and code availability
- **EXPERIMENTAL MODEL AND SUBJECT DETAILS**
 - *Xenopus laevis* frog maintenance and oocyte collection
- **METHOD DETAILS**
 - Materials
 - DNA constructs and RNA
 - HEK293T cell culture & transfection
 - BRET assay
 - Giant membrane patches (GMPs)
 - Confocal imaging
 - Computational modelling
 - Pulldown assay
 - Two electrode voltage clamp (TEVC)
 - Cell attached single channel recordings
- **QUANTIFICATION AND STATISTICAL ANALYSIS**

SUPPLEMENTAL INFORMATION

Supplemental information can be found online at <https://doi.org/10.1016/j.isci.2021.103018>.

ACKNOWLEDGMENTS

This work was supported by: Israel-India Binational grant (Israeli # ISF_2255_2015 and Indian # UGC-6-1/2016 (1C) (N.D. and A.K.B.); Israel Science Foundation grant # ISF_1282_2018 (N.D.); NIH grant # MH54137 (J.A.J) and NNF grant # NNF17OC0024830 (M.H.P.).

AUTHOR CONTRIBUTION

Conceptualization: H.P.R., D.Y., J.A.J. and N.D. Methodology: H.P.R., T.K.R., D.Y., M.H.P. and N.D. Formal Analysis: H.P.R., T.K.R., D.Y., G.T., B.S., M.H.P., S.C. and N.D. Investigation: H.P.R., T.K.R., D.Y., G.T., B.S., M.H., V.A.T., S.C. and N.D. Writing – Original Draft: H.P.R. Writing – Review & Editing: H.P.R., D.Y., D.B.G., J.A.J., A.K.B. and N.D. Visualization: H.P.R., D.Y., A.K.B., S.C. and N.D. Supervision: N.D., A.K.B., J.A.J. and D.B.G. Project Administration: H.P.R. and N.D. Funding Acquisition: N.D., A.K.B., J.A.J., M.H.P. and D.B.G.

DECLARATION OF INTERESTS

D.B.G. is a founder of and holds equity in Q State Biosciences and Praxis Therapeutics; holds equity in Apostle Inc., and serves as a consultant to AstraZeneca, Gilead Sciences, GoldFinch Bio and Gossamer Bio. Other authors declare no competing interests.

Received: May 24, 2021

Revised: August 4, 2021

Accepted: August 18, 2021

Published: September 24, 2021

REFERENCES

- Albsoul-Younes, A.M., Sternweis, P.M., Zhao, P., Nakata, H., Nakajima, S., Nakajima, Y., and Kozasa, T. (2001). Interaction sites of the G protein β subunit with brain G protein-coupled inward rectifier K^+ channel. *J. Biol. Chem.* 276, 12712–12717. <https://doi.org/10.1074/jbc.M011231200>.
- Bean, B.P. (1989). Neurotransmitter inhibition of neuronal calcium currents by changes in channel voltage dependence. *Nature* 340, 153–156. <https://doi.org/10.1038/340153a0>.
- Berg, J.M., Tymoczko, J.L., and Stryer, L. (2012). *With Gregory J. Gatto, Jr. Biochemistry, 7th ed. (W.H. Freeman)*.
- Berlin, S., Keren-Raifman, T., Castel, R., Rubinstein, M., Dessauer, C.W., Ivanina, T., and Dascal, N. (2010). $G\alpha_x$ and $G\beta\gamma$ jointly regulate the conformations of a $G\beta\gamma$ effector, the neuronal G protein-activated K^+ channel (GIRK). *J. Biol. Chem.* 285, 6179–6185. <https://doi.org/10.1074/jbc.M109.085944>.
- Berlin, S., Tsemakhovich, V.A., Castel, R., Ivanina, T., Dessauer, C.W., Keren-Raifman, T., and Dascal, N. (2011). Two distinct aspects of coupling between $G\alpha_x$ protein and G protein-activated K^+ channel (GIRK) revealed by fluorescently labeled $G\alpha_{x3}$ protein subunits. *J. Biol. Chem.* 286, 33223–33235. <https://doi.org/10.1074/jbc.M111.271056>.
- Betke, K.M., Wells, C.A., and Hamm, H.E. (2012). GPCR mediated regulation of synaptic

- transmission. *Prog. Neurobiol.* 96, 304–321. <https://doi.org/10.1016/j.pneurobio.2012.01.009>.
- Chan, K.W., Sui, J.-L., Vivaudou, M., and Logothetis, D.E. (1996). Control of channel activity through a unique amino acid residue of a G protein-gated inwardly rectifying K⁺ channel subunit. *Proc. Natl. Acad. Sci.* 93, 14193–14198. <https://doi.org/10.1073/pnas.93.24.14193>.
- Colombo, S., Petri, S., Shalomov, B., Reddy, H.P., Tabak, G., Dhindsa, R.S., Gelfman, S., Teng, S., Krizay, D., Rafikian, E.E., et al. (2019). G protein-coupled potassium channels implicated in mouse and cellular models of GNB1 Encephalopathy. *BioRxiv*, 697235. <https://doi.org/10.1101/697235>.
- Corey, S., and Clapham, D.E. (2001). The stoichiometry of Gβγ binding to G-protein-regulated inwardly rectifying K⁺ channels (GIRKs). *J. Biol. Chem.* 276, 11409–11413. <https://doi.org/10.1074/jbc.M100058200>.
- Dascal, N., and Lotan, I. (1992). Expression of exogenous ion channels and neurotransmitter receptors in RNA-injected *Xenopus* oocytes. In *Protocols in Molecular Neurobiology*, A. Longstaff and P. Revest, eds. (Springer New York), pp. 205–225. <https://doi.org/10.1385/0-89603-199-3:205>.
- Dascal, N., Schreimbayer, W., Lim, N.F., Wang, W., Chavkin, C., DiMaggio, L., Labarca, C., Kieffer, B.L., Gaveriaux-Ruff, C., Trollinger, D., et al. (1993). Atrial G protein-activated K⁺ channel: expression cloning and molecular properties. *Proc. Natl. Acad. Sci. United States America* 90, 10235–10239. <https://doi.org/10.1073/pnas.90.21.10235>.
- Dascal, N. (2001). Ion-channel regulation by G proteins. *Trends Endocrinol. Metab.* 12, 391–398. [https://doi.org/10.1016/S1043-2760\(01\)00475-1](https://doi.org/10.1016/S1043-2760(01)00475-1).
- Dascal, N., and Kahanovitch, U. (2015). The roles of Gβγ and Gα in gating and regulation of GIRK channels. *Int. Rev. Neurobiol.* 123, 27–85. <https://doi.org/10.1016/bs.irm.2015.06.001>.
- Deng, H., Xiu, X., and Song, Z. (2014). The molecular biology of genetic-based epilepsies. *Mol. Neurobiol.* 49, 352–367. <https://doi.org/10.1007/s12035-013-8523-6>.
- Dißmann, E., Wischmeyer, E., Spauschus, A., Pfeil, D., Karschin, C., and Karschin, A. (1996). Functional expression and cellular mRNA localization of a G protein-activated K⁺ inward rectifier isolated from rat brain. *Biochem. Biophysical Res. Commun.* 223, 474–479. <https://doi.org/10.1006/bbrc.1996.0918>.
- Dolphin, A.C. (2003). G protein modulation of voltage-gated calcium channels. *Pharmacol. Rev.* 55, 607–627. <https://doi.org/10.1124/pr.55.4.3>.
- Donthamsetti, P., Quejada, J.R., Javitch, J.A., Gurevich, V.V., and Lambert, N.A. (2015). Using bioluminescence resonance energy transfer (BRET) to characterize agonist-induced arrestin recruitment to modified and unmodified G protein-coupled receptors. *Curr. Protoc. Pharmacol.* 70, 2.14.1–2.14.14. <https://doi.org/10.1002/0471141755.ph0214s70>.
- Endo, W., Ikemoto, S., Togashi, N., Miyabayashi, T., Nakajima, E., Hamano, S.-I., Shibuya, M., Sato, R., Takezawa, Y., Okubo, Y., et al. (2020). Phenotype-genotype correlations in patients with GNB1 gene variants, including the first three reported Japanese patients to exhibit spastic diplegia, dyskinetic quadriplegia, and infantile spasms. *Brain & Development* 42, 199–204. <https://doi.org/10.1016/j.braindev.2019.10.006>.
- Ford, C.E., Skiba, N.P., Bae, H., Daaka, Y., Reuveny, E., Shekter, L.R., Rosal, R., Weng, G., Yang, C.S., Iyengar, R., et al. (1998). Molecular basis for interactions of G protein βγ subunits with effectors. *Science* 280, 1271–1274. <https://doi.org/10.1126/science.280.5367.1271>.
- Gomora, J.C., Daud, A.N., Weiergräber, M., and Perez-Reyes, E. (2001). Block of cloned human T-type calcium channels by succinimide antiepileptic drugs. *Mol. Pharmacol.* 60, 1121–1132.
- Guo, Y., Waldron, G.J., and Murrell-Lagnado, R. (2002). A role for the middle C terminus of G-protein-activated inward rectifier potassium channels in regulating gating. *J. Biol. Chem.* 277, 48289–48294. <https://doi.org/10.1074/jbc.M207987200>.
- Hedin, K.E., Lim, N.F., and Clapham, D.E. (1996). Cloning of a *Xenopus laevis* inwardly rectifying K⁺ channel subunit that permits GIRK1 expression of IK_{ACh} currents in oocytes. *Neuron* 16, 423–429. [https://doi.org/10.1016/s0896-6273\(00\)80060-4](https://doi.org/10.1016/s0896-6273(00)80060-4).
- Hemati, P., Revah-Politi, A., Bassan, H., Petrovski, S., Bilancia, C.G., Ramsey, K., Griffin, N.G., Bier, L., Cho, M.T., Rosello, M., et al. (2018). Refining the phenotype associated with GNB1 mutations: clinical data on 18 newly identified patients and review of the literature. *Am. J. Med. Genet. A* 176, 2259–2275. <https://doi.org/10.1002/ajmg.a.40472>.
- Hollins, B., Kuravi, S., Digby, G.J., and Lambert, N.A. (2009). The C-terminus of GRK3 indicates rapid dissociation of G protein heterotrimers. *Cell Signal.* 21, 1015–1021. <https://doi.org/10.1016/j.cellsig.2009.02.017>.
- Hu, C.-D., and Kerppola, T.K. (2003). Simultaneous visualization of multiple protein interactions in living cells using multicolor fluorescence complementation analysis. *Nat. Biotechnol.* 21, 539–545. <https://doi.org/10.1038/nbt816>.
- Huang, Y., Zhang, Y., Kong, S., Zang, K., Jiang, S., Wan, L., Chen, L., Wang, G., Jiang, M., Wang, X., et al. (2018). GIRK1-mediated inwardly rectifying potassium current suppresses the epileptiform burst activities and the potential antiepileptic effect of ML297. *Biomed. Pharmacother.* 101, 362–370. <https://doi.org/10.1016/j.biopha.2018.02.114>.
- Ikeda, S.R. (1991). Double-pulse calcium channel current facilitation in adult rat sympathetic neurones. *J. Physiol.* 439, 181–214. <https://doi.org/10.1113/jphysiol.1991.sp018663>.
- Ito, H., Tung, R.T., Sugimoto, T., Kobayashi, I., Takahashi, K., Katada, T., Ui, M., and Kurachi, Y. (1992). On the mechanism of G protein βγ subunit activation of the muscarinic K⁺ channel in Guinea pig atrial cell membrane. Comparison with the ATP-sensitive K⁺ channel. *J. Gen. Physiol.* 99, 961–983. <https://doi.org/10.1085/jgp.99.6.961>.
- Ivanova-Nikolova, T.T., and Breitwieser, G.E. (1997). Effector contributions to Gβγ-mediated signaling as revealed by muscarinic potassium channel gating. *J. Gen. Physiol.* 109, 245–253. <https://doi.org/10.1085/jgp.109.2.245>.
- Jeremic, D., Sanchez-Rodriguez, I., Jimenez-Diaz, L., and Navarro-Lopez, J.D. (2021). Therapeutic potential of targeting G protein-gated inwardly rectifying potassium (GIRK) channels in the central nervous system. *Pharmacol. Ther.* 223, 107808. <https://doi.org/10.1016/j.pharmthera.2021.107808>.
- Kahanovitch, U., Tsemakhovich, V., Berlin, S., Rubinstein, M., Styr, B., Castel, R., Peleg, S., Tabak, G., Dessauer, C.W., Ivanina, T., and Dascal, N. (2014). Recruitment of Gβγ controls the basal activity of G-protein coupled inwardly rectifying potassium (GIRK) channels: crucial role of distal C terminus of GIRK1. *J. Physiol.* 592, 5373–5390. <https://doi.org/10.1113/jphysiol.2014.283218>.
- Kanevsky, N., and Dascal, N. (2006). Regulation of maximal open probability is a separable function of Ca_vβ subunit in L-type Ca²⁺ channel, dependent on NH₂ terminus of α_{1C} (Cav1.2α). *J. Gen. Physiol.* 128, 15–36. <https://doi.org/10.1085/jgp.200609485>.
- Kaufmann, K., Romaine, I., Days, E., Pascual, C., Malik, A., Yang, L., Zou, B., Du, Y., Sliwoski, G., Morrison, R.D., et al. (2013). ML297 (VU0456810), the first potent and selective activator of the GIRK potassium channel, displays antiepileptic properties in mice. *ACS Chem. Neurosci.* 4, 1278–1286. <https://doi.org/10.1021/cn400062a>.
- Kessel, A., and Ben-Tal, N. (2018). *Introduction to Proteins Structure, Function, and Motion* (CRC Press, Taylor & Francis Group).
- Kobayashi, T., Hirai, H., Iino, M., Fuse, I., Mitsumura, K., Washiyama, K., Kasai, S., and Ikeda, K. (2009). Inhibitory effects of the antiepileptic drug ethosuximide on G protein-activated inwardly rectifying K⁺ channels. *Neuropharmacology* 56, 499–506. <https://doi.org/10.1016/j.neuropharm.2008.10.003>.
- Kozek, K.A., Du, Y., Sharma, S., Prael, F.J., 3rd, Spitznagel, B.D., Kharade, S.V., Denton, J.S., Hopkins, C.R., and Weaver, C.D. (2019). Discovery and characterization of VU0529331, a synthetic small-molecule activator of homomeric G Protein-gated, inwardly rectifying, potassium (GIRK) channels. *ACS Chem. Neurosci.* 10, 358–370. <https://doi.org/10.1021/acschemneuro.8b00287>.
- Krapivinsky, G., Gordon, E.A., Wickman, K., Velimirović, B., Krapivinsky, L., and Clapham, D.E. (1995). The G-protein-gated atrial K_{ACh} channel I_{KACH} is a heteromultimer of two inwardly rectifying K⁺-channel proteins. *Nature* 374, 135–141. <https://doi.org/10.1038/374135a0>.
- Laskowski, R.A., Jabłońska, J., Pravda, L., Vařeková, R.S., and Thornton, J.M. (2018). PDBsum: structural summaries of PDB entries. *Protein Sci.* 27, 129–134. <https://doi.org/10.1002/pro.3289>.
- Lodowski, D.T., Pitcher, J.A., Capel, W.D., Lefkowitz, R.J., and Tesmer, J.J.G. (2003). Keeping G proteins at bay: a complex between G protein-coupled receptor kinase 2 and Gβγ. *Science* 300, 1256–1262. <https://doi.org/10.1126/science.1082348>.

- Logothetis, D.E., Mahajan, R., and Adney, S.K. (2015). Unifying mechanism of controlling Kir3 channel activity by G proteins and phosphoinositides. *Int. Rev. Neurobiol.* 123, 1–26. <https://doi.org/10.1016/bs.im.2015.05.013>.
- Lohmann, K., Masuho, I., Patil, D.N., Baumann, H., Hebert, E., Steinrück, S., Trujillo, D., Skamangas, N.K., Dobricic, V., Hüning, I., et al. (2017). Novel GNB1 mutations disrupt assembly and function of G protein heterotrimers and cause global developmental delay in humans. *Hum. Mol. Genet.* 26, 1078–1086. <https://doi.org/10.1093/hmg/ddx018>.
- Luján, R., Marron Fernandez de Velasco, E., Aguado, C., and Wickman, K. (2014). New insights into the therapeutic potential of G_i channels. *Trends Neurosciences* 37, 20–29. <https://doi.org/10.1016/j.tins.2013.10.006>.
- Lüscher, C., and Slesinger, P.A. (2010). Emerging roles for G protein-gated inwardly rectifying potassium (GIRK) channels in health and disease. *Nat. Rev. Neurosci.* 11, 301–315. <https://doi.org/10.1038/nrn2834>.
- Mahajan, R., Ha, J., Zhang, M., Kawano, T., Kozasa, T., and Logothetis, D.E. (2013). A Computational Model Predicts that G $\beta\gamma$ acts at a cleft between channel subunits to activate GIRK1 channels. *Sci. Signaling* 6, ra69. <https://doi.org/10.1126/scisignal.2004075>.
- Mertz, C., Krarup, S., Jensen, C.D., Lindholm, S.E.H., Kjær, C., Pinborg, L.H., and Bak, L.K. (2020). Aspects of cAMP signaling in epileptogenesis and seizures and its potential as drug target. *Neurochem. Res.* 45, 1247–1255. <https://doi.org/10.1007/s11064-019-02853-x>.
- Mirshahi, T., Mittal, V., Zhang, H., Linder, M.E., and Logothetis, D.E. (2002). Distinct sites on G protein $\beta\gamma$ subunits regulate different effector functions. *J. Biol. Chem.* 277, 36345–36350. <https://doi.org/10.1074/jbc.M205359200>.
- Nishida, M., and MacKinnon, R. (2002). Structural basis of inward rectification: cytoplasmic pore of the G protein-gated inward rectifier GIRK1 at 1.8 Å resolution. *Cell* 111, 957–965. [https://doi.org/10.1016/s0092-8674\(02\)01227-8](https://doi.org/10.1016/s0092-8674(02)01227-8).
- Noebels, J. (2017). Precision physiology and rescue of brain ion channel disorders. *J. Gen. Physiol.* 149, 533–546. <https://doi.org/10.1085/jgp.201711759>.
- Oldham, W.M., and Hamm, H.E. (2006). Structural basis of function in heterotrimeric G proteins. *Q. Rev. Biophys.* 39, 117–166. <https://doi.org/10.1017/S0033583506004306>.
- Oldham, W.M., and Hamm, H.E. (2008). Heterotrimeric G protein activation by G-protein-coupled receptors. *Nat. Rev. Mol. Cell Biol.* 9, 60–71. <https://doi.org/10.1038/nrm2299>.
- Oz, S., Benmocha, A., Sasson, Y., Sachyani, D., Almagor, L., Lee, A., Hirsch, J.A., and Dascal, N. (2013). Competitive and non-competitive regulation of calcium-dependent inactivation in Ca_v1.2 L-type Ca²⁺ channels by calmodulin and Ca²⁺-binding protein 1. *J. Biol. Chem.* 288, 12680–12691. <https://doi.org/10.1074/jbc.M113.460949>.
- Petrovski, S., Kürty, S., Myers, C.T., Anyane-Yeboah, K., Cogné, B., Bialer, M., Xia, F., Hemati, P., Riviello, J., Mehaffey, M., et al. (2016). Germline de novo mutations in GNB1 cause severe neurodevelopmental disability, hypotonia, and seizures. *Am. J. Hum. Genet.* 98, 1001–1010. <https://doi.org/10.1016/j.ajhg.2016.03.011>.
- Pires, G., Leitner, D., Drummond, E., Kanshin, E., Nayak, S., Askenazi, M., Faustin, A., Friedman, D., Debure, L., Ueberheide, B., et al. (2021). Proteomic differences in the hippocampus and cortex of epilepsy brain tissue. *Brain Commun.* <https://doi.org/10.1093/braincomms/fcab021>.
- Pires, D.E.V., Ascher, D.B., and Blundell, T.L. (2014). mCSM: predicting the effects of mutations in proteins using graph-based signatures. *Bioinformatics (Oxford, England)* 30, 335–342. <https://doi.org/10.1093/bioinformatics/btt691>.
- Prelich, G. (2012). Gene overexpression: uses, mechanisms, and interpretation. *Genetics* 190, 841–854. <https://doi.org/10.1534/genetics.111.136911>.
- Revah-Politi, A., Sands, T.T., Colombo, S., Goldstein, D.B., and Anyane-Yeboah, K. (2020). GNB1 Encephalopathy. In *Gene Reviews [Internet]* (Seattle (WA): University of Washington), pp. 1993–2021.
- Richter, J.D., and Smith, L.D. (1981). Differential capacity for translation and lack of competition between mRNAs that segregate to free and membrane-bound polysomes. *Cell* 27, 183–191. [https://doi.org/10.1016/0092-8674\(81\)90372-x](https://doi.org/10.1016/0092-8674(81)90372-x).
- Rishal, I., Keren-Raifman, T., Yakubovich, D., Ivanina, T., Dessauer, C.W., Slepak, V.Z., and Dascal, N. (2003). Na⁺ promotes the dissociation between G α GDP and G $\beta\gamma$, activating G protein-gated K⁺ channels. *J. Biol. Chem.* 278, 3840–3845. <https://doi.org/10.1074/jbc.C200605200>.
- Rishal, I., Porozov, Y., Yakubovich, D., Varon, D., and Dascal, N. (2005). G $\beta\gamma$ -dependent and G $\beta\gamma$ -independent basal activity of G protein-activated K⁺ channels. *J. Biol. Chem.* 280, 16685–16694. <https://doi.org/10.1074/jbc.M412196200>.
- Rubinstein, M., Peleg, S., Berlin, S., Brass, D., and Dascal, N. (2007). G α i3 primes the G protein-activated K⁺ channels for activation by coexpressed G $\beta\gamma$ in intact *Xenopus* oocytes. *J. Physiol.* 581, 17–32. <https://doi.org/10.1113/jphysiol.2006.125864>.
- Rubinstein, M., Peleg, S., Berlin, S., Brass, D., Keren-Raifman, T., Dessauer, C.W., Ivanina, T., and Dascal, N. (2009). Divergent regulation of GIRK1 and GIRK2 subunits of the neuronal G protein-gated K⁺ channel by G α GDP and G $\beta\gamma$. *J. Physiol.* 587, 3473–3491. <https://doi.org/10.1113/jphysiol.2009.173229>.
- Sadana, R., and Dessauer, C.W. (2009). Physiological roles for G protein-regulated adenylyl cyclase isoforms: insights from knockout and overexpression studies. *NeuroSignals* 17, 5–22. <https://doi.org/10.1159/000166277>.
- Sadja, R., Alagem, N., and Reuveny, E. (2002). Graded contribution of the G $\beta\gamma$ binding domains to GIRK channel activation. *Proc. Natl. Acad. Sci. United States America* 99, 10783–10788. <https://doi.org/10.1073/pnas.162346199>.
- Sakmann, B., and Neher, E. (1995). *Single-Channel Recording* (Plenum Press).
- Shore, A.N., Colombo, S., Tobin, W.F., Petri, S., Cullen, E.R., Dominguez, S., Bostick, C.D., Beaumont, M.A., Williams, D., Khodagholy, D., et al. (2020). Reduced GABAergic neuron excitability, altered synaptic connectivity, and seizures in a *KCNT1* gain-of-function mouse model of childhood epilepsy. *Cell Rep* 33, 108303. <https://doi.org/10.1016/j.celrep.2020.108303>.
- Singer-Lahat, D., Dascal, N., Mittelman, L., Peleg, S., and Lotan, I. (2000). Imaging plasma membrane proteins in large membrane patches of *Xenopus* oocytes. *Pflügers Archiv Eur. J. Physiol.* 440, 627–633. <https://doi.org/10.1007/s004240050014>.
- Slesinger, P.A., Patil, N., Liao, Y.J., Jan, Y.N., Jan, L.Y., and Cox, D.R. (1996). Functional effects of the mouse weaver mutation on G protein-gated inwardly rectifying K⁺ channels. *Neuron* 16, 321–331. [https://doi.org/10.1016/s0896-6273\(00\)80050-1](https://doi.org/10.1016/s0896-6273(00)80050-1).
- Stevens, E.B., Woodward, R., Ho, I.H.M., and Murrell-Lagnado, R. (1997). Identification of regions that regulate the expression and activity of G protein-gated inward rectifier K⁺ channels in *Xenopus* oocytes. *J. Physiol.* 503, 547–562. <https://doi.org/10.1111/j.1469-7793.1997.547bg.x>.
- Tabak, G., Keren-Raifman, T., Kahanovitch, U., and Dascal, N. (2019). Mutual action by G γ and G β for optimal activation of GIRK channels in a channel subunit-specific manner. *Scientific Rep.* 9. <https://doi.org/10.1038/s41598-018-36833-y>.
- Tedford, H.W., and Zamponi, G.W. (2006). Direct G protein modulation of Ca_v2 calcium channels. *Pharmacol. Rev.* 58, 837–862. <https://doi.org/10.1124/pr.58.4.11>.
- Torkamani, A., Andersen, K.G., Steinhilb, S.R., and Topol, E.J. (2017). High-definition medicine. *Cell* 170, 828–843. <https://doi.org/10.1016/j.cell.2017.08.007>.
- Treiber, F., Rosker, C., Keren-Raifman, T., Steinecker, B., Gorischek, A., Dascal, N., and Schreibmayer, W. (2013). Molecular basis of the facilitation of the heterooligomeric GIRK1/GIRK4 complex by cAMP dependent protein kinase. *Biochim. Biophys. Acta - Biomembranes* 1828, 1214–1221. <https://doi.org/10.1016/j.bbame.2012.12.016>.
- Tselnicker, I., Tsemakhovich, V.A., Dessauer, C.W., and Dascal, N. (2010). Stargazin modulates neuronal voltage-dependent Ca²⁺ channel Ca_v2.2 by a G $\beta\gamma$ -dependent mechanism. *J. Biol. Chem.* 285, 20462–20471. <https://doi.org/10.1074/jbc.M110.121277>.
- Vivaudou, M., Chan, K.W., Sui, J.-L., Jan, L.Y., Reuveny, E., and Logothetis, D.E. (1997). Probing the G-protein regulation of GIRK1 and GIRK4, the two subunits of the K_{ACH} channel, using functional homomeric mutants. *J. Biol. Chem.* 272, 31553–31560. <https://doi.org/10.1074/jbc.272.50.31553>.
- Wall, M.A., Coleman, D.E., Lee, E., Iñiguez-Lluhi, J.A., Posner, B.A., Gilman, A.G., and Sprang, S.R. (1995). The structure of the G protein heterotrimer G α i1 β 1 γ 2. *Cell* 83, 1047–1058. [https://doi.org/10.1016/0092-8674\(95\)90220-1](https://doi.org/10.1016/0092-8674(95)90220-1).
- Wang, W., Touhara, K.K., Weir, K., Bean, B.P., and Mackinnon, R. (2016). Cooperative regulation by

G proteins and Na⁺ of neuronal GIRK2 K⁺ channels. *Elife* 5, e15751. <https://doi.org/10.7554/eLife.15751>.

Weaver, C.D., and Denton, J.S. (2021). Next-generation inward rectifier potassium channel modulators: discovery and molecular pharmacology. *Am. J. Physiol.* <https://doi.org/10.1152/ajpcell.00548.2020>.

Whorton, M.R., and MacKinnon, R. (2013). X-ray structure of the mammalian GIRK2-βγ G-protein complex. *Nature* 498, 190–197. <https://doi.org/10.1038/nature12241>.

Wickman, K., and Clapham, D.E. (1995). Ion channel regulation by G proteins. *Physiol. Rev.* 75, 865–885. <https://doi.org/10.1152/physrev.1995.75.4.865>.

Wydeven, N., Marron Fernandez De Velasco, E., Du, Y., Benneyworth, M.A., Hearing, M.C., Fischer, R.A., Thomas, M.J., Weaver, C.D., and Wickman, K. (2014). Mechanisms underlying the activation of G-protein-gated inwardly rectifying K⁺ (GIRK) channels by the novel anxiolytic drug, ML297. *Proc. Natl. Acad. Sci. United States America* 111, 10755–10760. <https://doi.org/10.1073/pnas.1405190111>.

Xue, L.C., Rodrigues, J.P., Kastiris, P.L., Bonvin, A.M., and Vangone, A. (2016). PRODIGY: a web server for predicting the binding affinity of protein-protein complexes. *Bioinformatics* (Oxford, England) 32, 3676–3678. <https://doi.org/10.1093/bioinformatics/btw514>.

Yakubovich, D., Berlin, S., Kahanovitch, U., Rubinstein, M., Farhy-Tselnicker, I., Styr, B., Keren-Raifman, T., Dessauer, C.W., and Dascal, N. (2015). A quantitative model of the GIRK1/2 channel reveals that its basal and evoked activities are controlled by unequal stoichiometry of Gα and Gβγ. *PLoS Comput. Biol.* 11. <https://doi.org/10.1371/journal.pcbi.1004598>.

Yakubovich, D., Pastushenko, V., Bitler, A., Dessauer, C.W., and Dascal, N. (2000). Slow modal gating of single G protein-activated K⁺ channels expressed in *Xenopus* oocytes. *J. Physiol.* 524, 737–755. <https://doi.org/10.1111/j.1469-7793.2000.00737.x>.

Yakubovich, D., Rishal, I., Dessauer, C.W., and Dascal, N. (2009). Amplitude histogram-based method of analysis of patch clamp recordings that involve extreme changes in channel activity levels. *J. Mol. Neurosci.* 37, 201–211. <https://doi.org/10.1007/s12031-008-9117-z>.

Yim, Y.Y., McDonald, W.H., Hyde, K., Cruz-Rodríguez, O., Tesmer, J.J.G., and Hamm, H.E. (2017). Quantitative multiple-reaction monitoring proteomic analysis of Gβ and Gγ subunits in C57Bl6/J brain synaptosomes. *Biochemistry* 56, 5405–5416. <https://doi.org/10.1021/acs.biochem.7b00433>.

Yoda, A., Adelmant, G., Tamburini, J., Chapuy, B., Shindoh, N., Yoda, Y., Weigert, O., Kopp, N., Wu, S.C., Kim, S.S., et al. (2015). Mutations in G protein β subunits promote transformation and kinase inhibitor resistance. *Nat. Med.* 21, 71–75. <https://doi.org/10.1038/nm.3751>.

Yokogawa, M., Osawa, M., Takeuchi, K., Mase, Y., and Shimada, I. (2011). NMR analyses of the Gβγ binding and conformational rearrangements of the cytoplasmic pore of G Protein-activated inwardly rectifying potassium channel 1 (GIRK1). *J. Biol. Chem.* 286, 2215–2223. <https://doi.org/10.1074/jbc.M110.160754>.

Zamponi, G.W., and Currie, K.P.M. (2013). Regulation of Cav2 calcium channels by G protein coupled receptors. *Biochim. Biophys. Acta* 1828, 1629–1643. <https://doi.org/10.1016/j.bbame.2012.10.004>.

Zamponi, G.W., Striessnig, J., Koschak, A., and Dolphin, A.C. (2015). The physiology, pathology, and pharmacology of voltage-gated calcium channels and their future therapeutic potential. *Pharmacol. Rev.* 67, 821–870. <https://doi.org/10.1124/pr.114.009654>.

Zhao, Y., Ung, P.M.-U., Zadoránszky-Kóhalmi, G., Zakharov, A.V., Martínez, N.J., Simeonov, A., Glaaser, I.W., Rai, G., Schlessinger, A., Marugan, J.J., and Slesinger, P.A. (2020). Identification of a G-protein-independent activator of GIRK channels. *Cell Rep.* 31, 107770. <https://doi.org/10.1016/j.celrep.2020.107770>.

Zimmermannova, O., Doktorova, E., Stuchly, J., Kanderova, V., Kuzilkova, D., Strnad, H., Starkova, J., Alberich-Jorda, M., Falkenburg, J.H.F., Trka, J., et al. (2017). An activating mutation of GNB1 is associated with resistance to tyrosine kinase inhibitors in ETV6-ABL1-positive leukemia. *Oncogene* 36, 5985–5994. <https://doi.org/10.1038/ncr.2017.210>.

STAR★METHODS

KEY RESOURCES TABLE

REAGENT or RESOURCE	SOURCE	IDENTIFIER
Antibodies		
Donkey IgG (1:200)	Jackson ImmunoResearch	017-000-003; RRID:AB_2337256; Lot 131795
GNB1	GeneTex	GTX114442; RRID:AB_10619473; Lot 43565
Rabbit polyclonal anti-G β (T-20) (1:500)	Santa Cruz Biotechnology	sc-378; RRID:AB_631542; currently discontinued
Goat Anti-Rabbit IgG H&L– DyLight649 (1:400)	SeraCare (KPL)	072-08-18-06; currently discontinued
Goat Anti-Rabbit IgG H&L– DyLight650 (1:200)	Abcam	ab96886; RRID:AB_10680254; Lot GR3228258-6
Bacterial strains		
DH5 α	New England Biolabs	C29871
One Shot MAX Efficiency DH5 α -T1 ^R	ThermoFisher	12297016
Chemicals, peptides, and recombinant proteins		
VU0529331	Alomone labs	V-155
ML297	Alomone labs	M-215
Barium Chloride (BaCl ₂)	Merck	1719.0500
Potassium chloride (KCl)	Merck	1.04936.1000
Sodium chloride (NaCl)	Merck	1.06404.1000
Magnesium chloride (MgCl ₂ .6H ₂ O)	Merck	1.05833.1000
Calcium Chloride (CaCl ₂)	Sigma-Aldrich	C1016
HEPES	Biological industries	41-122-100
Sodium Hydroxide (NaOH)	Merck	1.06498.1000
Potassium Hydroxide (KOH)	Merck	1.05033.1000
Methanesulfonic acid	Sigma-Aldrich	471356
Barium Hydroxide (Ba(OH) ₂)	Sigma-Aldrich	B2507
Collagenase-Type 1A	Sigma-Aldrich	C9891-1G
Na-Pyruvate	Sigma-Aldrich	P2256
Gentamycin Sulfate Solution, 50mg/ml	Biological industries	03-035-1b
Dulbecco's Phosphate Buffered Saline (DPBS)*Without Calcium and Magnesium	Biological industries	02-023-1A
SeaKem LE Agarose	Lonza	50004
Delbeco's Phosphate buffer saline (D-PBS)	Corning	#21-031-CV
Formaldehyde solution, ACS reagent, 37 wt. % in H ₂ O, contains 10-15% Methanol as stabilizer (to prevent polymerization)	Sigma-Aldrich	252549
Difco skim milk	BD	232100
Dulbecco's Modified Eagle Medium (DMEM)	Gibco	11965-092
L- Glutamine	Corning	25-005-CI
fetal bovine serum (FBS)	Corning	35-010
Trypsin EDTA	Gibco	25300-054
Pen Strep	Corning	30-002
Poly-L-lysine	Sigma-Aldrich	P2636
Ampicillin	Sigma-Aldrich	A9518
Glucose	Sigma-Aldrich	G8270
coelenterazine H	Dalton	50909-86-9

(Continued on next page)

Continued

REAGENT or RESOURCE	SOURCE	IDENTIFIER
dopamine hydrochloride	Sigma-Aldrich	H-8502
Acetylcholine	Sigma-Aldrich	A6625
Sylgard	DOW CORNING	182 Curing agent; 182 silicone elastomer
Superdex 75 column	GE Healthcare	17-1044-01
glutathione sepharose beads	GE Healthcare	17-0756-01
Rabbit reticulocyte lysate	Promega	L4960
[³⁵ S]-methionine	PerkinElmer	NEG 772002MC
Lubrol	ICN Biomedicals	195299
Tris HCL (Trizma Base)	Sigma	T1503
SDS	Sigma	L3771
glycerol	Bio-Lab	0007 12050100
2- mercaptoethanol	Aldrich	M6250
acrylamide	Bio-Rad	1610156

Critical commercial assays

GeneArt Site-directed Mutagenesis Plus System	ThermoFisher	A14604
QIAprep Spin Miniprep Kit	Qiagen	27106
Miniprep Kit	Promega	A1460
PWO master PCR	Roche	03789403001
polyethylenimine	Polysciences	23966-2
REAGENT or RESOURCE	SOURCE	IDENTIFIER
Nhe1	New England Biolabs	R3131S
Sall	New England Biolabs	R3138S

Experimental models: cell lines

HEK293T cells	ATTC	CRL-1573
Xenopus laevis oocytes	Xenopus-1	http://www.xenbase.org/community/org.do?orgId=1365&method=Display

Oligonucleotides

GIRK5 antisense oligonucleotide 5'T*A*AAT*CCC* TTG*CCA*TGA*T*G*G*T-3'	HyLabs	Custom oligonucleotide
DNA primers for mutagenesis	This study	
K78R Fwd: 5'-CCTCGCAGGATGGTAGACT TATCATCTGGGA-3' Rev: 5'-TCCCAGATGATA AGTCTACCATCCTGCGAGG-3'	HyLabs	Custom primer
I80N Fwd: 5'-AGGATGGTAACTTAACATC TGGGACAGCTA-3' Rev: 5'-TAGCTGTCC CAGATGTTAAGTTTACCATCCT-3'	HyLabs	Custom primer
I80T Fwd: 5'-AGGATGGTAACTTACC ATCTGGGACAGCTA-3' Rev: 5'-TAGCTGT CCCAGATGGTAAAGTTTACCATCCT-3'	HyLabs	Custom primer

Recombinant DNA

Rat GIRK1	(Dascal et al., 1993)	NP_113798.1
Rat YFP-GIRK1	(Berlin et al., 2010)	N/A
Rat GIRK1 _{F137S} GIRK1*	(Yakubovich et al., 2000)	N/A
Mouse GIRK2	(Slesinger et al., 1996)	NP_001020755.1
Mouse GIRK2-YFP	(Yakubovich et al., 2000)	N/A
Human GIRK2	Blavatnik center, TAU	NM_002240

(Continued on next page)

Continued

REAGENT or RESOURCE	SOURCE	IDENTIFIER
Rat GIRK3	(Dißmann et al., 1996)	NP_446286.1
Rat GIRK4	(Krapivinsky et al., 1995)	NP_058993.1
Human G α i3 (C351I)	(Berlin et al., 2010)	single site mutation (C351I) of NP_006487.1
Bovine G β 1 WT	Melvin Simon, Caltech, USA	NP_786971.2
Bovine G β 1 D76G	This work	
Bovine G β 1 K78R	This work	
Bovine G β 1 I80N	This work	
Bovine G β 1 I80T	This work	
Bovine G β 1 M101V	This work	
Bovine G γ 2	Melvin Simon, Caltech, USA	P63212.2
Human M2R	EG Peralta, Harvard University, USA	NP_001006631.1
<i>Bordetella pertussis</i> PTX-A (S1 subunit)	Eitan Reuveny, Weizmann Institute, Israel	CAB51543.1
GST-G1NC _{short}	Dascal Lab	
GST-G1NC _{long}	Craig Douppnik, University of South Florida, USA	
GST-G2NC	(Kahanovitch et al., 2014) Dascal Lab	
Human dopamine 2 receptor short isoform (D2R)	(Donthamsetti et al., 2015)	
Human G α 1	cDNA.org	
Human G α oA	cDNA.org	
masGRKct-Rluc8	Nevin Lambert, Augusta University, USA	
venus156-239-G β 1WT (V2- β 1)	Cathy Berlot, Yale University, USA	
venus156-239-G β 1K78R (V2- β 1)	This work	
venus156-239-G β 1I80N (V2- β 1)	This work	
venus156-239-G β 1I80T (V2- β 1)	This work	
venus1-155-G γ 2 (V1- γ 2)	Cathy Berlot, Yale University, USA	
Software and algorithms		
Prism 9	GraphPad	https://www.graphpad.com/scientific-software/prism/
SigmaPlot 11 or 13	Systat Software, Inc.	https://systatsoftware.com/products/sigmaplot/sigmaplot-version-13/
pClamp 10.5	Molecular Devices	https://www.moleculardevices.com
BioRender 2021	BioRender	https://biorender.com/
Zeiss LSM5 image browser	EAMNET	https://www.embl.de/eamnet/html/body_image_browser.html
PRODIGY	(Xue et al., 2016)	https://bianca.science.uu.nl/prodigy/
PDBsum	(Laskowski et al., 2018)	http://www.ebi.ac.uk/thorntonsrv/databases/cgi-bin/pdbsum/GetPage.pl?pdbcode=index.html
MCSM server	(Pires et al., 2014)	http://biosig.unimelb.edu.au/mcsm/
ImageJ	NIH	https://imagej.nih.gov/ij/
ImageQuant 5.2	GE healthcare	
Other		
Axopatch 200B	Molecular Devices	https://www.moleculardevices.com
Geneclamp 500	Molecular Devices	https://www.moleculardevices.com
PherastarFS	BMG Labtech	https://www.bmglabtech.com/pherastar-fsx/

RESOURCE AVAILABILITY

Lead contact

Further information and requests for resources and reagents should be directed to and will be fulfilled by the Lead Contact, Nathan Dascal (dascaln@tauex.tau.ac.il).

Materials availability

For this study we have generated single-site mutations in bovine G β ₁ cDNA inserted into the pGEM-HJ vector, suitable for RNA production for *Xenopus* oocyte experiments. These sequences are not unique (single or double nucleotide mutants) and have not been deposited in Addgene. Plasmids generated in this study are fully available without any restrictions upon request to the lead contact.

Data and code availability

No unique datasets or codes have been generated. The data reported in this paper are fully presented in the text, figures and the Table. Any additional information required to reanalyze the data reported in this paper is available from the lead contact upon request.

EXPERIMENTAL MODEL AND SUBJECT DETAILS

Xenopus laevis frog maintenance and oocyte collection

Experiments have been approved by, and conducted in accordance with instructions of, Tel Aviv University Institutional Animal Care and Use Committee (permits #01-16-104 and 01-20-083). Female *Xenopus laevis* frogs were maintained and operated, and oocyte defolliculation, incubation and RNA injection were performed as described previously (Dascal and Lotan 1992). Frogs were housed in dechlorinated water tanks and maintained on a 10 h light/14 h dark cycle at $19 \pm 2^\circ\text{C}$. Portions of ovary were removed through a small incision on the abdomen of frog under anesthesia (0.17% solution of methanesulphonate). After suturing the incision, frog was held in a separate tank to fully recover from the anesthesia and then shifted to post-operational animals' tank. The frogs did not show any signs of post-operational distress and were allowed to recover for at least three months. After four to five surgeries, anaesthetized frogs were killed by decapitation and double pithing.

Oocytes were defolliculated with collagenase (Type 1A, Sigma) in Ca-free ND96 solution. After 2-4 h of shaking incubation, oocytes were washed and placed in a petri dish with fresh ND-96 in the incubator for overnight. Next day, healthy looking oocytes were sorted into fresh dish and maintained in the incubator in NDE solution (ND96 solution supplemented with 2.5 mM pyruvate and 50 $\mu\text{g}/\text{ml}$ gentamicin) at 20°C until RNA injection or further use by giving a change of solution once a day. RNA injection was performed as described previously (Rubinstein et al., 2009). Healthy oocytes were injected with 50 nl of RNA and incubated for 2-4 days in NDE solution. The standard ND96 solution contained (in mM): 96 NaCl, 2 KCl, 1 MgCl₂, 1 CaCl₂, 5 HEPES, and was titrated with NaOH to pH of 7.6- 7.8. CaCl₂ was omitted in Ca²⁺-free ND96.

METHOD DETAILS

Materials

All materials are listed in the Key Resources Table.

DNA constructs and RNA

DNA constructs used for BRET assay were expressed in the pcDNA3.1+ vector (Invitrogen, Carlsbad, CA). Human dopamine 2 receptor short isoform (D2R) had a signal peptide (MKTIIALSIFYCLVFA) and FLAG (ADYKDDDDA) tag attached to the N-terminus. Human G α_{i1} and G α_{oA} were from cdna.org. The luciferase donor was Rluc8 fused to the membrane tethered C-terminus of GPCR kinase 3 that binds to G β ₃ (masGRKct-Rluc8) and the acceptor was a split-Venus fused to G γ 2 an G β ₁ as follows; Venus1-155-G γ 2 (V1- γ 2) and Venus156-239-G β ₁ (V2- β 1)(Hollins et al., 2009). Donor and acceptor constructs were a generous gift from Dr. Nevin Lambert (MCG, Augusta, GA).

To create the mutant *GNB1* constructs for the BRET assay, site-directed mutagenesis was performed on the pcDNA3.1+ Venus156-239-G β ₁ (V2- β 1) plasmid using the GeneArt Site-directed Mutagenesis Plus System (ThermoFisher #A14604). DNA was extracted using the QIAprep Spin Miniprep Kit (Qiagen #27106).

DNA constructs used to perform experiments in *Xenopus* oocytes were cloned into high expression oocyte vectors pGEM-HE or pGEM-HJ as described previously (Berlin et al., 2011; Rishal et al., 2005). Most DNA constructs were as reported previously: bovine G β ₁, bovine Gy2, human muscarinic type 2 receptor (M2R), human G α i3C_{351L}, Pertussis toxin protomer-A (PTX), rat GIRK1, mouse GIRK2, human GIRK2, YFP-GIRK1 (rat), mouse GIRK2-YFP, GIRK3 (rat), GIRK4 (rat) (Berlin et al., 2011; Rishal et al., 2003; Rubinstein et al., 2009; Treiber et al., 2013). PCR-site directed mutagenesis was performed on bovine G β ₁ to generate GNB1 point mutations - G β 1_{K78R}, G β 1_{I80N} and G β 1_{I80T} using standard procedures with the PWO master PCR kit (Roche # 03789403001). DNAs were prepared using the Wizard® Plus SV Miniprep kit (Promega # A1460). RNA was synthesized *in vitro* as described previously (Rishal et al., 2003). Amounts of injected RNA are indicated in the text and in Figure legends.

HEK293T cell culture & transfection

HEK293T cells were grown in Dulbecco DMEM + GlutaMAX™-I (Gibco, Invitrogen, Paisley, UK) with 10% fetal bovine serum (Corning #35-010) and 1% penicillin/streptomycin (Corning #30-002) at 37°C with 5% CO₂. For BRET assay preparation the cells were washed with D-PBS (Corning #21-031-CV), detached with 0.05% trypsin-EDTA (Gibco #25300-054) and seeded at 400 K cells/well in a 12-well format (Falcon #353043). The cells were transfected the following day with the following DNA concentrations; 150 ng D2R, 40 ng masGRKct-Rluc8, 200 ng V1- γ 2, 200 ng V2- β 1 WT/K78R/I80N/I80T, 300 ng G α _{OA/i1} and 443 ng pcDNA3.1+ to reach a final concentration of 1333 ng DNA/well. Cells were transfected with poly-ethylenimine (PEI; linear, MW 25,000; Polysciences, cat. No. 23966-2) at a 1:1 ratio (PEI: DNA) in growth medium overnight. The following day media was exchanged to fresh growth media.

BRET assay

Day 2 post transfection the cells were washed with D-PBS, detached, and resuspended in 500 μ l D-PBS + 5 mM glucose. HEK293T cells were seeded at 50 μ l/well into a 96-well black-white iso plate (PerkinElmer) and incubated with 5 μ M coelenterazine H (10 μ l/well) for 5 min before addition of 40 μ l/well of dopamine hydrochloride (Sigma-Aldrich #H-8502) to achieve a final concentration of 10 μ M. BRET was measured 2 min after dopamine addition using a PherastarFS (BMG Labtech) plate reader with detection filters set for 485 nM (Rluc8) and 525 nM (Venus). The BRET ratio was calculated for each well as (acceptor fluorescence)/(donor fluorescence). Agonist-induced BRET was calculated by subtracting BRET_{dopamine} - BRET_{vehicle}. Raw data were imported into GraphPad Prism 9 for analysis.

Giant membrane patches (GMPs)

Giant membrane patches of oocyte membrane were prepared and imaged as described (Kahanovitch et al., 2014; Singer-Lahat et al., 2000). Oocytes were manually devitellinized using fine forceps in a hypertonic solution (in mM: NaCl 6, KCl 150, MgCl₂ 4, HEPES 10, pH 7.6). The devitellinized oocytes were transferred onto a Thermanox™ coverslip (Nunc, Roskilde, Denmark) immersed in a Ca²⁺-free ND96 solution, with their animal pole facing the coverslip, for 10–20 minutes. The oocytes were then suctioned using a Pasteur pipette, leaving a giant plasma membrane patch attached to the coverslip, with the cytosolic face toward the external medium. The coverslip was washed thoroughly with fresh ND96 solution and fixed using 4% formaldehyde for 30 minutes. Fixed giant PM patches were immunostained in 5% milk in phosphate buffer solution (PBS). Non-specific binding was blocked with Donkey IgG 1:200 (Jackson ImmunoResearch, West Grove, PA, USA). Rabbit anti-G β (T-20) antibody (Santa Cruz Biotechnology, sc-378; discontinued currently) (Figures 1A and 1E), or rabbit anti-G β ₁ antibody (Abcam, ab 137635) (Figure S1) were applied at 1:500 or 1:300 dilution respectively, for 45 min at 37°C. DyLight 649-labeled secondary antibody- Goat Anti-rabbit IgG (1:400; SeraCare (KPL), 072-08-18-06; discontinued currently) (Figures 1A and 1E) or DyLight 650-labeled secondary antibody- Goat Anti-rabbit IgG (1:200; Abcam, ab 96886) (Figure S1) was then applied for 30 minutes in 37°C, washed with PBS, and mounted on a slide for visualization. Immunostained slides were kept in 4°C for no more than a week.

Confocal imaging

Confocal imaging and analysis were performed as described (Berlin et al., 2011; Kahanovitch et al., 2014) with a Zeiss 510 META confocal microscope, using a 20x objective. In whole oocytes, the image was focused on oocyte's animal (dark) hemisphere, at the equator. Images were acquired using spectral (λ)-mode: YFP was excited with the 514 nm line of the argon laser and emission was collected at 535–546 nm. Fluorescent signals were averaged from 3 regions of interest (ROI) at the PM and 3 similar ROIs from the coverslip

outside the oocyte's image, using Zeiss LSM Image Browser. The average background signal was subtracted from the average PM signal in each oocyte, and then the average net signal from the membrane of uninjected (naïve) oocytes was subtracted as well.

Imaging of proteins in giant PM patches (GMPs) was performed using the confocal microscope in λ -mode as described (Tabak et al., 2019). DyLight 649 or DyLight 650 was excited using 633 nm laser and emission was collected at 663–673 nm. Images centered on edges of the membrane patches, so that background fluorescence from coverslip could be seen and subtracted. Two ROIs were chosen: one comprising most of the membrane patch within the field of view, and another comprising background fluorescence, which was subtracted from the signal obtained from the patch. The signal from giant PM patches of native oocytes' membranes, immunostained using the same protocol, was subtracted from all groups.

Computational modelling

Three structure models were used: GIRK2-G β complex (crystal structure, protein databank accession number: 4kfm published by Whorton and MacKinnon (2013) and 2 models of GIRK1-G β complex (docking models developed by Mahajan et al. (2013): best scoring model -bs and largest cluster-lc. PDB files were analyzed in PRODIGY <https://bianca.science.uu.nl/prodigy/> (Xue et al., 2016) and interface residues graphs were generated. In each graph, number of amino acids in contact is plotted versus corresponding residue of G β . Interface amino acids data were obtained from affinity analysis conducted by PRODIGY server (which defines protein-protein interface as residues at 5.5 Å and below distance from each other). Similar results were obtained when analyzing protein complexes by PDBsum <http://www.ebi.ac.uk/thorntonsrv/databases/cgibin/pdbsum/GetPage.pl?pdbcode=index.html> (Laskowski et al., 2018). Subsequently, structural models were submitted to MCSM server <http://biosig.unimelb.edu.au/mcsm/> for estimation of folding energy changes expected by each mutation (Pires et al., 2014). We classified mutations as significantly influencing GIRK-G β interaction in case $\Delta\Delta G$ was larger than 1 kcal/mole, which corresponds to ~ 5 fold change in dissociation constant at 25°C (Berg et al., 2012) (~ 0.6 kcal/mole is considered noise threshold (Kessel and Ben-Tal, 2018).

Pulldown assay

Glutathione-S-transferase (GST)-fused constructs of GIRK1 and GIRK2 contained the cytosolic N and C-terminal domains, the transmembrane domain was replaced by a 2–6 a.a. linker. The DNA constructs were cloned into the pGEX-4T-1 vector (Amersham). GST-G1NC_{short} and GST-G2NC were made in the lab using standard PCR-based procedures. The GST-G1NC_{short} contained the rat GIRK1 sequence GIRK1 identical to that used for the crystallization of the GIRK1 cytosolic domain (Nishida and MacKinnon, 2002) a.a. 41–63, 190–371, connected by a 2 a.a. linker Lys-Leu. The GST-G2NC protein contained the mouse GIRK2A sequence, a.a. 1–94, 195–414, connected by a 2 a.a. linker Lys-Ser (Kahanovitch et al., 2014). The GST-G1NC_{long} was a generous gift from Craig Doupnik (University of South Florida). It contained the rat GIRK1 sequence, a.a. 1–84, 184–501 connected by a Hi₆ linker (Berlin et al., 2011). All GST-fused proteins were produced in *E. coli* and purified on a glutathion affinity column as described (Rishal et al., 2003), followed by size exclusion chromatography separation on a Superdex 75 column (GE Healthcare).

Pull down experiments were conducted essentially as described (Berlin et al., 2011; Kahanovitch et al., 2014). GST-fused proteins were pulled-down using glutathione sepharose beads (GE healthcare). In four experiments, *in vitro* translated (ivt) [³⁵S]-methionine – labeled G β (wt and mutants) and G γ were co-translated in rabbit reticulocyte lysate (Promega, #L4960). In four additional experiments the ivt proteins were not labeled with [³⁵S]-methionine, in which case protein detection on gels was performed using Western blots. 3 to 10 μ l of the lysate containing the ivt proteins were mixed with GST or one of the purified GST-fused GIRK cytosolic domain proteins in incubation buffer (150 mM KCl, 1 mM EDTA, 5 mM MgCl₂, 0.01% Lubrol, 50 mM Tris HCl pH 7.6; final volume 300 μ l per reaction). The mixture was incubated while shaking for 1 hour at room temperature, then 30 μ l glutathione sepharose beads were added, and incubated for 30 min at 4°C. The beads were washed 3 times with 500 μ l incubation buffer. For elution, the incubation buffer was removed, 20 μ l of 2X Laemmli buffer (8% SDS, 40% glycerol, 20% 2-mercaptoethanol, 0.008% bromophenol blue and 0.25 M Tris HCl, pH 6.8.) were added, followed by heating for 5 min at 95°C and centrifugation for 2 min at 50 g. The supernatant was collected and 20 μ l of water were added and loaded on 12% gel for separation by sodium dodecyl sulfate polyacrylamide gel electrophoresis (SDS-PAGE). 1/60 of the mixture before the pull-down was also loaded, usually on a separate gel ("input"). Gels of the [³⁵S]-methionine-labeled proteins were dried and imaged using Sapphire™ Biomolecular

Imager (Azure Biosystems, Dublin, CA, USA). For non-radioactive gels, we prepared Western blots using standard procedures using the primary rabbit anti-G β (T-20) antibody (as for GMPs but at 1:200) and secondary peroxidase-conjugated anti-rabbit IgG (Jackson ImmunoResearch 1:40000. #111-035-144). Autoradiograms and Western blots were analyzed using ImageQuant 5.2 (GE healthcare) or ImageJ (<https://imagej.nih.gov/ij/>). Binding was calculated as percent of input and then normalized to the binding of the control wt G $\beta\gamma$ construct used in the same experiment.

Two electrode voltage clamp (TEVC)

All experiments were performed at 20–22°C essentially as described (Rubinstein et al., 2009). Currents were recorded at –80 mV, filtered at 500 Hz, and sampled at 5 or 10 kHz. Whole-cell GIRK and Cav3.2 currents in oocytes were measured using two-electrode voltage clamp (TEVC) with Geneclamp 500 (Molecular Devices, Sunnyvale, CA, USA), using agarose cushion electrodes filled with 3M KCl, with resistances of 0.1–0.8 M Ω for current electrode and 0.2–1.5 M Ω for voltage electrode. To measure GIRK currents by direct activation by G $\beta\gamma$, oocytes were injected with RNAs of- GIRK1 and GIRK2 (0.05 ng) or GIRK2 (2 ng) or GIRK1 and GIRK3 (3 ng) or GIRK1 and GIRK4 (1 and 0.5 ng) or GIRK4 (5 ng) and the indicated amounts of G β RNA. The amount of G γ RNA was 1/5 of G β . To achieve approximately equal molar ratios of G β and G γ RNAs, we used RNA ratios of 5:1 or 5:2 for G β :G γ . Currents via GIRK channels were measured in ND96 solution or high-K⁺ solution (HK24), in mM: 24 KCl, 72 NaCl, 1 CaCl₂, 1 MgCl₂ and 5 HEPES. I_{basal} was measured after blocking all GIRK currents by 1 mM Ba²⁺ (Rubinstein et al., 2007). To measure GIRK currents activated through M2R, oocytes were injected with RNAs of GIRK1 and GIRK2 (0.02 or 0.1 ng) or GIRK2 (5 or 10 ng); M2R (0.1–0.5 ng); PTX (1 or 2 ng); G α i3_{C3511} (2.5 or 5 ng) and the indicated amounts of G β RNA (WT or mutant). The amount of G γ RNA was 1/5 or 2/5 of G β . Currents via GIRK channels were measured in ND96 solution or high-K⁺ solution (HK24) or HK24+ACh (10 μ M) solution. I_{evoked} or I_{ACh} was measured after blocking total GIRK currents by 1 mM Ba²⁺ and subtracting I_{basal} from total currents, I_{total} ($I_{\text{total}} = I_{\text{basal}}$ and I_{ACh} ; $I_{\text{ACh}} = I_{\text{total}} - I_{\text{basal}}$). pH of all solutions was 7.4–7.6. To measure Cav3.2 currents, oocytes were injected with equal amounts, usually 1 ng, of RNAs of Cav2.2 (α 1B), α 2 δ and Ca ν β _{2b} subunits of Ca²⁺ channels (Tselnicker et al., 2010) with or without G $\beta\gamma$ (5 ng G β and 1 or 2 ng G γ or G γ -YFP). Currents via Cav2.2 were measured in Ca²⁺-free extracellular solution with 5 (or 40 mM) Ba²⁺: 5 (or 40) mM Ba(OH)₂, 85 (or 50) mM NaOH, 2 mM KOH, and 5 mM HEPES, titrated to pH 7.5 with methanesulfonic acid (Tselnicker et al., 2010). The facilitation was measured in 40 mM Ba²⁺ solution using the protocol shown in Figure 3D.

VU0529331 (Alomone Labs; V-155) was dissolved in 100% DMSO to a final concentration of 25 mM. To measure GIRK2 response to VU0529331, the drug was diluted into HK24 solution to 2.5, 10 and 40 μ M concentrations. ML297 (Alomone Labs; M-215) was dissolved in 100% DMSO to a final concentration of 25 mM. To measure GIRK1/3 response to ML297, the drug was diluted into HK24 solution to 2.5, 10 and 40 μ M concentrations.

Cell attached single channel recordings

Patch clamp experiments were performed using Axopatch 200B (Molecular Devices, Sunnyvale, CA) as described (Yakubovich et al., 2015). Currents were recorded at –80 mV, filtered at 2 kHz and sampled at 20 kHz. Patch pipettes had resistances of 1.4–3.5 MO. Pipette solution contained, in mM: 144 KCl, 2 NaCl, 1 MgCl₂, 1 CaCl₂, 1 GdCl₃, 10 HEPES/KOH, pH 7.5. GdCl₃ completely inhibited the stretch-activated channels. The bath solution contained, in mM: 144 KCl, 2 MgCl₂, 6 NaCl, 1 EGTA, 10 HEPES/KOH, pH 7.5. To obtain single channel recordings, oocytes were injected with low doses of RNA of GIRK1 (10–50 pg), and RNA of GIRK2 was 1/2 to 1/3 of that (5–17 pg), to avoid the formation of GIRK2 homotetramers. For GIRK2 homomeric single channels recording, RNA injected was 25–50 pg and the indicated amounts of G β RNA. The amount of G γ RNA was 1/5 of G β . In addition, 25 ng of the antisense oligonucleotide against oocyte's endogenous GIRK5 was injected to prevent the formation of GIRK1/5 channels (Hedin et al., 1996). Single channel current (i_{single}) was calculated from all-point histograms of the original records (Yakubovich et al., 2009, 2015), and open probability (P_o) was obtained from event lists generated using idealization procedure based on 50% crossing criterion (Sakmann and Neher, 1995). Number of channels was estimated from overlaps of openings during the whole time of recording (at least 5 min). P_o was calculated only from records that contained up to 3 channels. Thus, the probability of missing a channel was negligible.

QUANTIFICATION AND STATISTICAL ANALYSIS

Statistical analysis was performed using SigmaPlot 11 or 13 (Systat Software, Inc.) and GraphPad Prism version 9 for Windows (GraphPad Software, La Jolla California USA). When summarizing imaging data

on protein expression or GIRK currents collected from several experiments, the results were normalized as described previously (Kanevsky and Dascal, 2006). Fluorescence intensity or current in each oocyte was normalized to the average signal in the oocytes of the control group of the same experiment. This procedure yields average normalized intensity or current, as well statistical variability (e.g., SEM), in all treatment groups as well as in the control group. Two-group comparisons were performed using t-test if the data passed the Shapiro-Wilk normality test and the equal variance test, otherwise we used the Mann-Whitney Rank Sum Test. Multiple group comparisons were done using one-way ANOVA (ANOVA on ranks was performed whenever the data did not distribute normally). Tukey's or Dunnett's tests were performed for normally distributed data and Dunn's or Kruskal-Wallis test otherwise. The data in the graphs are presented as mean \pm SEM, or as box plots, with all data points shown. Boxes show 25th and 75th percentiles and whiskers show minimal and maximal values; the horizontal line inside the box shows the median. Statistical differences are denoted as follows: asterisks (*) show comparison between Channel with WT G β and mutant groups; octothorpe sign (#) shows comparison with the Channel alone (no G $\beta\gamma$) group and G $\beta\gamma$ groups. * or #, $p < 0.05$; ** or ##, $p < 0.01$; *** or ###, $p < 0.001$; **** or ####, $p < 0.0001$.